Review

Design and Development of Photocatalytic Systems for Reduction of CO$_2$ into Valuable Chemicals and Fuels

Amra Bratovčić [1],* and Vesna Tomašić [2],*

[1] Department of Physical Chemistry and Electrochemistry, Faculty of Technology, University of Tuzla, Urfeta Vejzagića 8, 75000 Tuzla, Bosnia and Herzegovina

[2] Faculty of Chemical Engineering and Technology, University of Zagreb, Marulićev trg 19, 10000 Zagreb, Croatia

* Correspondence: amra.bratovcic@untz.ba (A.B.); vtomas@fkit.hr (V.T.)

Abstract: This review presents the results of research in the field of photocatalytic reduction of carbon dioxide (CO$_2$) to methane and methanol as valuable chemicals and fuels. CO$_2$ reduction is a promising technology, but it is an endothermic process with unfavourable thermodynamics. Other limitations include the inertness of the CO$_2$ molecule, the slow multielectron process, and the lack of understanding of the reaction mechanism, leading to low selectivity and insufficient efficiency. Tailoring reaction parameters such as CO$_2$ adsorption, choice of reducing agent, development of photocatalysts in terms of composition, structural properties and morphology, energy band gap, and the presence of surface functional groups can affect the reaction mechanism and selectivity for the desired product. Therefore, the main challenges in this research area are the development of an active and selective catalyst for the photoreduction of CO$_2$ to useful products with high added value and the optimization and development of a suitable photoreactor that allows successful contact between all key participants in the photocatalytic process. This review is intended to provide guidance for the future development of advanced photocatalysts and photocatalytic systems for CO$_2$ reduction and to enable further breakthroughs in this field.

Keywords: photocatalytic CO$_2$ reduction; efficiency; selectivity; methane; methanol; MOFs; semiconductor; TiO$_2$; Z-scheme heterojunction

1. Introduction

In recent years, and especially since the beginning of the war between Russia and Ukraine, the whole world is facing an energy crisis. Despite the constant development and increasing use of renewable energy sources (wind power, solar panels, and hydroelectric power plants), this political crisis has revealed Europe's great dependence on gas supplies from Russia. In addition, the increasing number of people on Earth leads to higher global energy demand. The use of excess fossil fuels for energy production is causing severe global warming and energy shortages. Therefore, the excessive emission of carbon dioxide (CO$_2$) from fossil-fuel combustion is a global issue that greatly influences climate change [1]. Global CO$_2$ emission from coal and fossil energy combustion and industrial processes has increased by 6% to 36.3 Gt from 2020 to 2021 [2]. The energy sector is the largest contributor to total CO$_2$ emissions in the European Union (EU-27) in 2020, with 30%, followed by transport with 27%, and industry at about 24% of total emissions, while other sectors contribute to a lesser extent [3]. Total national greenhouse-gas emissions in the United States were estimated to be 5.981 million metric tons of CO$_2$ in 2020 [4].

CO$_2$ belongs to the group of greenhouse gases (GHG) that trap heat and make the planet warmer. It contributes to over 60% of global warming [5]. Three basic approaches have been developed to reduce CO$_2$ emissions to the environment: (i) reducing CO$_2$ emissions at the source, (ii) CO$_2$ capture and storage (CCS), and (iii) reusing CO$_2$ by its conversion into useful carbon-containing products. CO$_2$ is a cheap, nontoxic, and abundant

C_1 feedstock for the production of alcohols, acids, and other value-added chemicals [6]. According to some expectations, the future "CO_2 economy" will probably be based on the conversion of CO_2 into fuels (methane, methanol, dimethyl ether, and gasoline/diesel/aviation fuel) and chemical intermediates (methane, methanol, etc.). In addition, CO_2 can serve as a feedstock for the synthesis of urea (for nitrogen fertilizers and plastics), salicylic acid (as a pharmaceutical ingredient), polycarbonates (plastics), and building materials (aggregates, cement, and concrete) [7,8] (Figure 1).
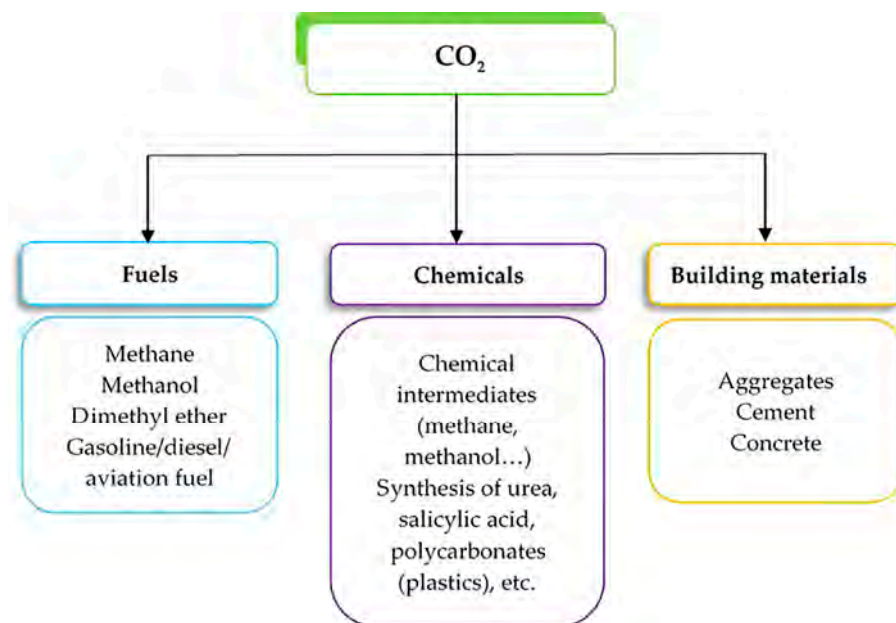

Figure 1. CO_2 conversion into useful carbon-containing products.

The aim of this review paper is to provide an overview of photocatalytic CO_2 conversion into high-value fuels and chemicals. The focus is on the development of promising photocatalysts responsible for the selectivity and efficiency of CO_2 photoreduction to C_1 products, a basic understanding of the reaction mechanism, and an overview of different photoreactor configurations.

2. Fundamentals of CO_2 Photoconversion

2.1. General Considerations

Interest in research on the photocatalytic conversion of CO_2 has steadily increased over the past decade, but the number of available scientific and review papers indicates that the field has not yet been adequately explored. Recently, photocatalysis has received increasing attention due to its green and sustainable features in energy and environmental issues. In particular, the photocatalytic conversion of CO_2 into value-added products is an attractive strategy to alleviate the energy crisis and reduce atmospheric CO_2 emissions. Therefore, the solar light-induced production of fuels and chemicals from the photochemical conversion of CO_2 and earth-abundant substances without any chemical reagents and external power inputs is an urgent need for carbon-neutral activities and renewable energy sources. Moreover, photocatalytic CO_2 conversion can be carried out at lower temperatures and pressures, decreasing energy consumption. The advantage of solar-based remediation technology is that it can be ideally suited for self-standing small-scale systems that can operate even in locations that are not connected to the electrical power grid [9]. The reduction of CO_2 can lead to a variety of carbon products, ranging from carbon monoxide and methane to higher hydrocarbons in the gas phase, as well as various oxygenates in the liquid phase, such as methanol and formic acid [10].

The photocatalytic strategy is of great practical value for CO_2 reduction by using clean and renewable solar energy to produce value-added products [11]. The wavelength range

of sunlight is mainly between 250 and 2500 nm, with ultraviolet light accounting for only 5%, visible light accounting for 43%, and near-infrared light accounting for 52% of the entire solar spectrum [12]. The photocatalytic CO_2 conversion into the desired products involves not only the usual steps for the catalytic reaction (adsorption, activation, and reaction at the catalyst surface) but also additional steps, such as the absorption of incident photons, and the generation, separation, and transfer of electron-hole pairs, e^--h^+. After absorption of the light irradiation, the photogenerated e^--h^+ pairs separate and migrate to the active sites on the surface, which usually occurs in a time of a few hundred picoseconds. Simultaneously with the charge transfer, charge recombination can occur in a time range from picoseconds to tens of nanoseconds, which is comparable to or faster than the charge-transfer process. Therefore, an innovative photocatalyst design is required to solve the problems related to the band-gap energy, charge transfer, and inhibition of photocatalytic reaction due to charge recombination.

Photocatalytic performances of photocatalysts are mainly determined by the efficiency of light utilization, charge transfer, and surface reaction. Semiconductor materials have received great attention and have shown good performance for CO_2 reduction. The most commonly used materials for the photocatalytic reduction of CO_2 are, variously, doped materials, such as TiO_2, WO_3, $g-C_3N_4$, and perovskites [13]. The most important technical issue for scientists is always efficiency. The efficiency of the above-mentioned materials is mainly determined by the band gap energy, charge separation, and charge transfer, which can be improved by doping, introducing defects (such as oxygen vacancies or geometric effects), cocatalysts, or using Z-scheme catalysts. In addition to the above materials ZnO, CdS, GaP, SiC [14], $BiVO_4$, [15], indium oxide (In_2O_3) [16], cerium oxide (CeO_2) [17], etc. are also investigated. Among all the semiconductor materials studied, TiO_2 has been widely explored as a photocatalyst for CO_2 reduction due to its suitable electronic/optical properties, low-cost availability, thermal stability, low toxicity, and high photoactivity.

From the thermodynamic point of view, the photocatalytic reduction of CO_2 can occur when the energy of the photocatalyst conduction band (CB) is more negative than the reduction potential of CO_2 to allow the transfer of electrons from the photocatalyst to the CO_2. On the other hand, to allow the oxidation of water or hydrogen molecules (reducing agents), the energy of the valence band (VB) needs to be more positive than the reduction potential of the reactants, allowing the transfer of holes from the catalyst to the reagents. The energy level at the bottom of the conduction band corresponds to the reduction potential of the photo-generated electrons, while the energy at the top of the valence band corresponds to the oxidation capability of the photo-generated holes (Figure 2) [18–21]. Thus, depending on the position of these energy levels, the semiconductor will be able to perform oxidation and/or reduction.

2.2. Modification of Existing Semiconductor Photocatalysts for Increasing Efficiency and Selectivity

Due to its higher band gap (3.20 eV for anatase), TiO_2 is only active when irradiated with UV light with a wavelength less than 380 nm [22]. Therefore, to overcome the strong limitation of its UV response, various modification techniques have been employed in the last few years. Photocatalytic reactions such as organic transformations, water splitting, and CO_2 reduction represent promising reactions for converting solar energy into chemical or thermal energy through light–matter interaction. The main problem of the insufficient utilization of sunlight in these conversions is a large energy band gap, fast charge recombination, and limited exposure of the photocatalyst active sites. Different modification strategies have been employed to reduce the energy band gap of pristine metal oxides, including ionic-ionic doping [23], metal modification [24] and nonmetal doping, heterojunction building [25] and oxygen vacancy creation [26], nanocarbons [27], graphene [28], enzymes [29], and novel sensitizers [30]. Inspired by natural photosynthesis, the artificial Z-scheme of the photocatalyst was constructed to provide a simple method to enhance the efficiency of CO_2 reduction [31]. In order to improve the adsorption and activation of CO_2,

the surface area of the photocatalyst must be increased (by tailoring its structure) through a controlled-synthesis process. The second strategy implies the introduction of surface defects (e.g., oxygen and sulphur vacancies), surface basic sites, and noble-metal cocatalysts. Furthermore, to increase the selectivity of the photoreduction toward the desired product, it is also necessary to know or predict the reaction mechanism [32].
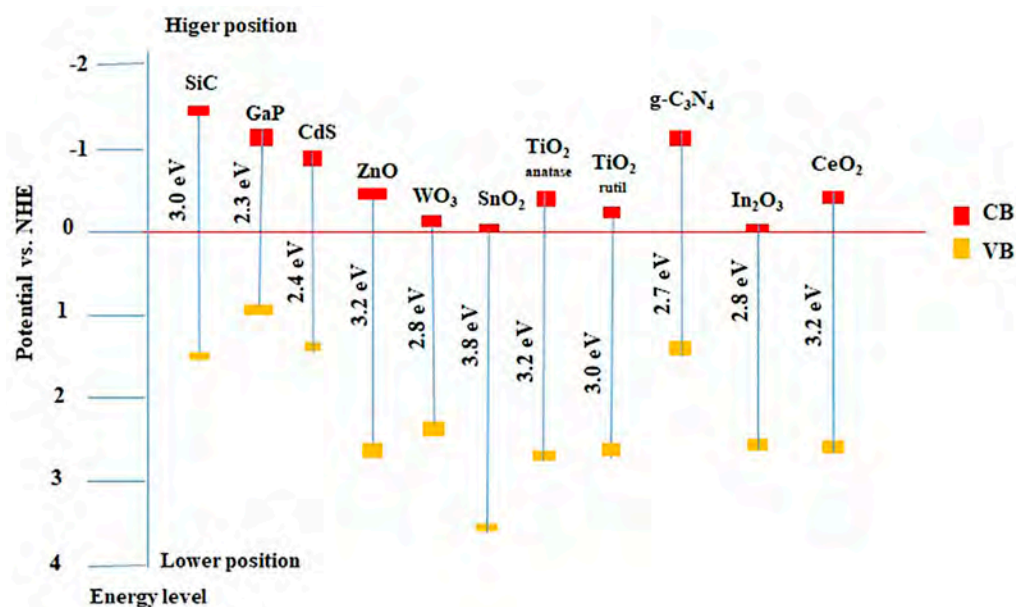

Figure 2. Schematic diagram of CB potentials of semiconductors of various semiconductors measured at pH 7 [18–21].

In order to improve the selectivity of photocatalytic CO_2 reduction to solar fuels using semiconductor catalysts, various modification strategies of cocatalysts preparation were employed [33]. The overall photoconversion efficiency and CO_2 reduction selectivity depend on light harvesting and charge separation, as well as the adsorption/activation of CO_2 molecules on the surface of the heterogeneous catalysts [32]. In addition to the control of light harvesting and charge transfer, the design of catalytically active sites is of great importance in promoting CO_2 reduction activity and selectivity (e.g., C–C coupling) [34]. It has been shown that the change of polycrystalline Ag nanoparticles to a single crystal structure can reduce CO selectivity in the photocatalytic conversion of CO_2 to CO by H_2O as an electron donor when Ag-loaded $NaTaO_3$ is used as a photocatalyst [35]. In this study, larger silver nanoparticles have a higher CO selectivity, while the photodeposition time was used to control the nanoparticle size. For stable and selective CO production in this reaction, a chromium shell was introduced in the core–shell structure of Ag-Cr on the surfaces of $NaTaO_3$.

In the Z-scheme photocatalytic system, which is usually composed of two photocatalysts with narrow bandgaps, the reaction involves two steps of photoexcitation (Figure 3) [36]. In the first, the electrons in the VB of photocatalyst I (PC I) are excited into its CB under sunlight, while the electrons in the VB of PC II are excited into its CB. After that, the photogenerated electrons in the CB of PC I are transferred to the VB of photocatalyst II and recombined with holes (PC I). Therefore, the photogenerated electrons in the CB of PC II are responsible for the reduction of CO_2, while oxidation of H_2O to O_2 and H^+ is carried out on the photogenerated holes in the VB of PC I. An illustration of this approach and promoting charge separation by constructing Z-scheme heterojunctions is given later in the chapter dealing with the review of photocatalysts for CO_2 reduction.
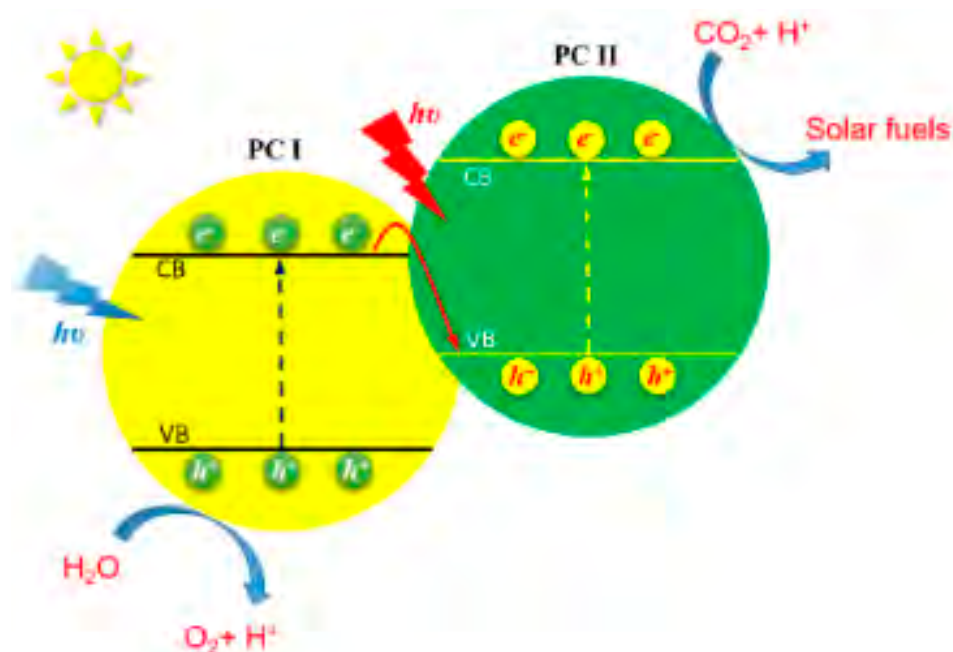
Figure 3. Charge transfer in a Z-scheme photocatalytic system (Reproduced from [36] Chao Peng, Glenn Reid, Haifeng Wang, P. Hu; perspective: photocatalytic reduction of CO_2 to solar fuels over semiconductors. *J. Chem. Phys.* 21 July 2017; 147 (3): 030901. https://doi.org/10.1063/1.4985624, Figure 13, with the permission of AIP Publishing).

2.3. Effect of Reductant and Sacrificial Agents on CO_2 Photoreduction

The mechanism of photocatalytic CO_2 reduction, the overall efficiency, and the distribution of the products depend significantly on the reducing agent and reaction medium used, and there are significant differences between water (H_2O), methanol (CH_3OH), methane (CH_4), and hydrogen (H_2) that can be used as possible reductants when the process is carried out in the liquid and/or gas phase [13,37].

Since the first report by Inoue et al. [38], liquid-phase systems have been extensively investigated. In the liquid-phase reaction system, the reduction of CO_2 is carried out with a saturated aqueous solution of CO_2. Water is the most common source of electrons and protons for the photocatalytic reduction of CO_2, due to its great availability, inexpensiveness, and environmental friendliness. However, H_2O as a solvent for this reaction suffers from a low CO_2 solubility, which hinders the interaction of CO_2 with the catalyst dispersed in the reaction medium. Therefore, in the last decade, gas-phase reactions using water vapour and/or hydrogen produced with renewable energy became more and more popular. Depending on the source and availability of protons and electrons, different products can be formed. The photocatalytic reduction of CO_2 by water mainly leads to the formation of C_1 products (methanol, methane, formaldehyde, formic acid, and carbon monoxide) and C_{2+} products (ethanol, ethylene, ethane, acetaldehyde, acetic acid, and oxalic acid) [39]. It is important to emphasize that in traditional systems the undesirable reduction of H_2O to H_2 can occur as a competitive reaction to CO_2 reduction, which seriously reduces the CO_2 conversion efficiency and limits the selectivity of products. This influence is much weaker in the gas–solid reaction system, due to the lower H_2O vapour content. Moreover, the gas–solid reaction systems have recently been favoured because they are more promising in terms of tuning reaction activity and selectivity in the photocatalytic reduction of CO_2.

Reduction of CO_2 by H_2 to hydrocarbons such as carbon monoxide, methane, methanol, dimethyl ether, long-chain hydrocarbons (lower olefins, gasoline, and aromatics), etc. is a very promising route to obtain value-added products. Since no oxygen can be formed during the hydrogenation of CO_2, the conversions are somewhat higher than when water is used as a reducing agent. Additional advantages of the gas–solid reaction system include easier mixing of reactants, the ability to optimize the CO_2/H_2O ratio, as well as the ability

to perform the reaction at higher CO_2 pressures, which improves the CO_2 adsorption on the surface of the photocatalyst [40]. Unfortunately, the photocatalytic reduction of CO_2 using H_2 has been largely neglected, so more attention needs to be paid to this topic.

The greatest opportunity is in the production of C_1 products, although C_{2+} are more desirable due to their higher market price (USD 1.0–4.5/kg) [11]. Among C_1 products, there is a particular interest in the production of methanol—the heart of the so-called "methanol economy" [8]. The formation of C_{2+} is limited by a large kinetic barrier that must be overcome for the formation of appropriate C-C bonds and unwanted competitive reactions [41]. Promoters, active metals, and supports that adjust the surface H/C ratio also play a very important role in achieving selectivity toward the desired product [42].

In addition to water (H_2O), methanol (CH_3OH), methane (CH_4), and hydrogen (H_2), other compounds such as sodium hydroxide (NaOH), ethanol (C_2H_5OH), propanol (C_3H_7OH), etc. were also used during the CO_2 photoreduction [43]. Although water is the most environmentally friendly solvent, naturally available in large quantities and a source of hydrogen, the disadvantage of its use as a solvent is the low solubility of the CO_2 molecule (2g L^{-1}) [44]. Therefore, a good solvent, instead of water, should allow higher solubility of CO_2, be cheaper and not degrade under irradiation conditions. In this sense, acetonitrile (C_2H_3N), ethyl acetate ($C_4H_8O_2$), aqueous solutions of carbonates and aqueous solutions of sodium hydroxide (NaOH) were investigated, also including several holes scavengers, such as triethanol amine (TEOA), triethyl amine (TEA), ethanol, etc. [45]. However, it is observed that both the organic substances involved in the preparation of the photocatalysts and the decomposition products of sacrificial reagents and/or reaction additives may decompose to small molecules, such as H_2, CO, and CH_4, causing the overestimation of catalytic activities or false positive results [46]. Unfortunately, such an important factor is sometimes overlooked in the desire to achieve the highest possible photocatalyst efficiency [47].

Liu et al. studied the role of solvents on product selectivity for CO_2 reduction [48]. They found that the use of solvents with low dielectric constants, such as carbon tetrachloride (CCl_4) and dichloromethane (CH_2Cl_2), led to $CO_2^{\bullet-}$ anion radicals being strongly absorbed on Ti sites due to the anions showing little solubility in these solvents of low polarity and, therefore, CO was the major product observed during this reaction [48]. However, when a high dielectric solvent such as H_2O was used, $CO_2^{\bullet-}$ anion radicals were greatly stabilized by the solvents which led to weak interactions with the surface of the photocatalyst, and thus formate ($HCOO^-$) was observed, as the main product via the reaction of a proton with the carbon atom of the $CO_2^{\bullet-}$ anion radical.

When hydrogen is used as a reductant, from the process point of view, it should be supplied in a sustainable form, e.g., as blue hydrogen (from steam reforming with CCS) or as green hydrogen (from water electrolysis) [49].

Depending on the choice of photocatalyst and reducing agent, as well as the reaction conditions, the most common products of CO_2 reduction include carbon monoxide (CO), methane (CH_4), and methanol (CH_3OH) (Figure 4, Table 1). The electrons in the conduction band of the photocatalyst are responsible for the reduction and conversion of adsorbed CO_2 to the desirable product, and the type of the product depends on the number of electrons available for the reactions.

Olivo et al. [40] performed an extensive experimental study of CO_2 photoreduction in both the liquid and gas phases under specific operating conditions optimized for both modes to investigate the influence of the reaction medium on process activity and selectivity and to determine the reaction mechanism. Based on experimental observations, they concluded that the choice of reaction medium (e.g., liquid phase vs. vapour phase) significantly affects the reaction mechanism as well as the product distribution. It was found that rapid deoxygenation occurs in the gas-phase mode, leading to the formation of the most reduced product (methane) as the dominant product. This is particularly evident in gas-phase reaction systems under conditions of excess CO_2, where the reaction mechanism involves the formation of C radicals that react with H originating from water vapour. On

the other hand, the same researchers point out that in the liquid phase, due to the higher H_2O/CO_2 molar ratio, hydrogenation proceeds faster than oxygenation, leading to the formation of C products such as CH_3OH, $HCOOH$, and $HCHO$, which are formed together with H_2. Therefore, the aforementioned researchers have shown that better performance in CO_2 photoreduction is achieved with liquid-phase CO_2 photoreduction, but under the condition of sufficiently high solubility of CO_2 at high pressure. Several works demonstrate that when water vapour or gaseous H_2 is the hydrogen source, the observed major product is either CH_4 or CO, whereas if liquid H_2O is used, the predominant reduced products are usually CH_3OH, $HCOOH$, or $HCHO$, as shown in Figure 4. On the other hand, in multiphase gas–liquid–solid systems, a combination of liquid and gaseous reductant (H_2O and H_2) is often used, resulting in the formation of various products such as CH_4, CH_3OH, $HCOOH$, and so on.
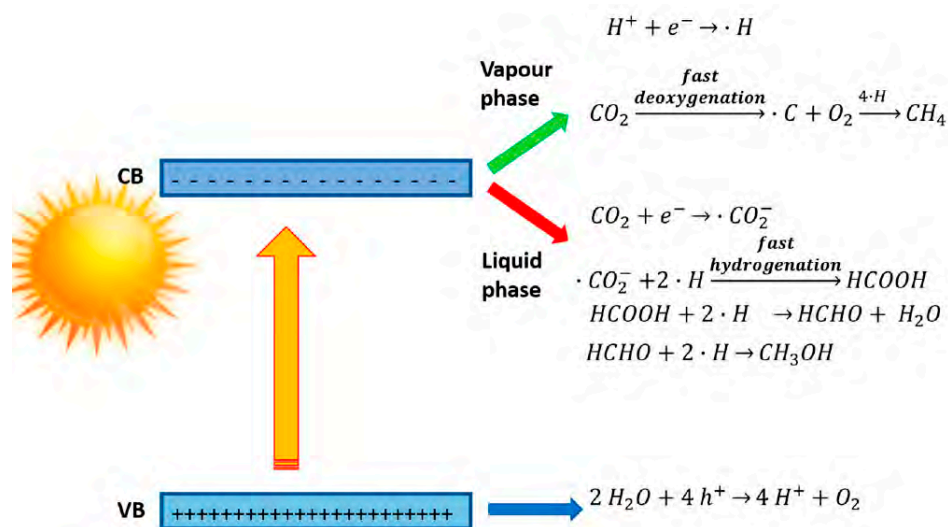

Figure 4. Process activity and selectivity in the vapour and liquid phase (Reproduced from [40], Figure 6, Alberto Olivo, Elena Ghedini, Michaela Signoretto, Matteo Compagnoni, Ilenia Rossetti, Liquid vs. Gas Phase CO_2 Photoreduction Process: Which Is the Effect of the Reaction Medium? *Energies.* **2017**, *10*, 1394).

Table 1. Electrochemical redox potentials for half-reactions at pH = 7 in an aqueous solution vs. the NHE. Reprinted from [18] with permission from Elsevier.

Ordered Number	Chemical Equation	Electrochemical Redox Potential (V) vs. NHE
1	$CO_2 + e^- \rightarrow CO_2^{\cdot-}$	−2.0
2	$2H^+ + 2e^- \rightarrow H_2$	−0.41
3	$CO_2 + 2H^+ + 2e^- \rightarrow HCOOH$	−0.61
4	$CO_2 + 4H^+ + 4e^- \rightarrow HCHO + H_2O$	−0.52
5	$CO_2 + 2H^+ + 2e^- \rightarrow CO + H_2O$	−0.48
6	$CO_2 + 6H^+ + 6e^- \rightarrow CH_3OH + H_2O$	−0.38
7	$CO_2 + 8H^+ + 8e^- \rightarrow CH_4 + 2H_2O$	−0.24
8	$H_2CO_3 + 2H^+ + 2e^- \rightarrow HCOOH + H_2O$	−0.166
9	$H_2CO_3 + 4H^+ + 4e^- \rightarrow HCHO + 2H_2O$	−0.050
10	$H_2CO_3 + 6H^+ + 6e^- \rightarrow CH_3OH + 2H_2O$	+0.044
11	$2CO_3^{2-} + 4H^+ + 2e^- \rightarrow C_2O_4^{2-} + 2H_2O$	+0.478
12	$2CO_3^{2-} + 3H^+ + 2e^- \rightarrow HCOO^- + 2H_2O$	+0.311
13	$2CO_3^{2-} + 8H^+ + 6e^- \rightarrow CH_3OH + 2H_2O$	+0.209
14	$2C_2O_4^{2-} + 2H^+ + 2e^- \rightarrow 2HCOO^-$	+0.145
15	$HCOO^- + 5H^+ + 4e^- \rightarrow CH_3OH + 2H_2O$	+0.157

2.4. Mechanism of the Photocatalytic CO_2 Reduction

The mechanism of photocatalytic CO_2 reduction by heterogeneous photocatalysts is a rather complex process, as it involves several steps, and different pathways are possible, leading to the formation of different products.

In general, CO_2 photoconversion involves the adsorption of gaseous CO_2, activation of adsorbed CO_2, formation of intermediates, and desorption of the products. This is followed by light absorption and electron-hole pair generation, charge carrier migration and spatial separation, and photocatalytic reactions at the photocatalyst surface. Separated electrons and holes (e^-/h^+) can also recombine at the surface (surface recombination) or in the volume of the semiconductor (volume recombination). Photogenerated electrons may arrive at the photocatalyst surface and be trapped by the adsorbed species (CO_2 and H_2O). A reduction reaction can occur at the surface when the photocatalyst donates an electron to reduce the CO_2 acceptor to various hydrocarbon products. On the other hand, a hole can be transferred to the surface where an electron from H_2O as a donor species undergoes an oxidation reaction to form (H_2) or OH radical and H^+. In other words, the reduction half reaction must be accompanied by an oxidation half reaction, such as H_2O oxidation. As mentioned previously, CO_2 reduction can be carried out in both the solution and gas phases. In particular, the process involves two major steps, the splitting of water to obtain hydrogen, which in turn helps in the reduction of carbon dioxide to different hydrocarbon products in the second step [50].

Methanol is the desired product in photocatalytic CO_2 reduction applications since it can be directly used as a liquid fuel instead of gasoline and diesel. The fact is that eight electrons (8 e^-) are required for the photoreduction of CO_2 to methane, while six electrons (6 e^-) are required for methanol (Table 1) [18,51]. To avoid the recombination of surface electrons with surface holes, electron donors should be added to consume the surface holes. The electron donors mainly include H_2O, methanol, or other sacrificial agents (e.g., triethanolamine (TEOA) and triethylamine (TEA), etc.). An important indicator that the electrons in the reaction originate from water and not from the sacrificial reagents is the production of a stoichiometric amount of O_2. The photocatalyst particles are not consumed during irradiation and therefore can be reused for several cycles until the active surface is blocked by the accumulation of organic matter [52]. In addition, the fundamental processes that could occur on the semiconductor must be considered to evaluate the potential product formation. Therefore, during the photocatalytic reduction of CO_2, it can be assumed that the following reactions occur from the point of view of thermodynamic reduction potential vs. standard hydrogen electrodes (NHE) [53–55] (see Table 1).

As can be seen from Table 1, the reduction potentials for the formation of methanol is -0.38 V and for methane is -0.24 V. Thus, when the reduction potential of the reaction is lower than the conductance band of the semiconductor, the photoexcited electrons can be used efficiently [56].

To increase the solubility of CO_2 in water, the photocatalytic reaction is usually carried out under basic pH values. In this way, the formation of carbonates and bicarbonates is inevitable, which act as lummy hole quenchers and contribute to favouring the oxidation reaction over reduction. On the other hand, a higher proton concentration favours the process of water-splitting, so that H_2 is produced faster than CO_2 is reduced. In addition, at a lower pH, the reduction of CO_2 to methanol can occur. In general, it is thermodynamically required that the relative potential of the acceptor (CO_2 and H_2O) be more positive than the conduction band of the adsorbent (semiconductor) for semiconductors to undergo photoinduced electron transfer to adsorbed species [18].

The carbene pathway and the formaldehyde pathway are two commonly recognized mechanisms for the photocatalytic CO_2 conversion described in the literature (Figure 5).
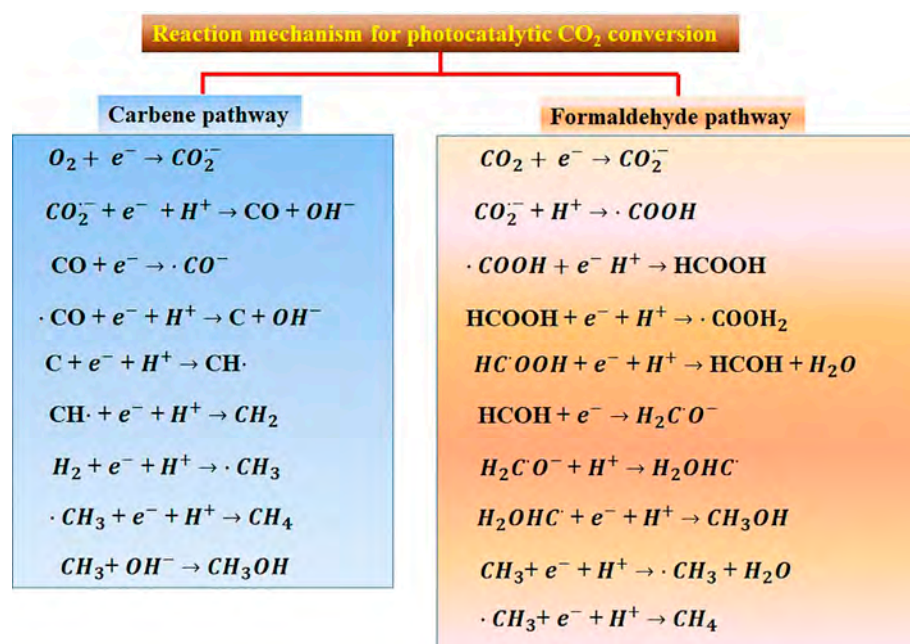
Figure 5. The carbene and the formaldehyde pathways for photocatalytic CO_2 conversion [57].

CO_2 reduction proceeds much more easily in the presence of reducing agents such as water (in a liquid or gaseous state) and hydrogen. Here, of course, water has an advantage over hydrogen because it is cheaper and readily available, and also less dangerous. When the photocatalyst is irradiated with a light irradiation energy greater than or equal to the band-gap energy of the semiconductor ($h\nu \geq E_g$), photoactivation occurs, resulting in the formation of electron-hole pairs (e^--h^+). The photoinduced electrons (e^-) move to the outer surface of the photocatalyst where CO_2 was previously adsorbed, leading to the formation of $\cdot CO_2^-$(ad) [57]. The next step is the process of oxidation of water. It takes place when a photogenerated hole reacts with water (reducing agent) to form a hydroxyl radical ($\cdot OH$) and a positive hydrogen ion (H^+). H^+ reacts with an electron to form a hydrogen radical ($\cdot H$). Then, the adsorbed anionic radical $\cdot CO_2^-$(ad) reacts with the hydrogen radical ($\cdot H$) to form carbon monoxide (CO) and a hydroxyl ion (OH^-). Carbon monoxide (CO) reacts with an electron to form the CO anionic radical ($\cdot CO^-$), which reacts with the hydrogen radical ($\cdot H$) to form the carbon radical ($\cdot C$) and a hydroxyl ion (OH^-). The resulting carbon radical ($\cdot C$) reacts with a hydrogen radical ($\cdot H$) to form a CH radical ($\cdot CH$), which in turn reacts with a hydrogen radical ($\cdot H$) to form a CH_2 radical ($\cdot CH_2$), which in turn reacts with the hydrogen radical ($\cdot H$) to form the CH_3 radical ($\cdot CH_3$). In the formation of the methyl radical ($\cdot CH_3$), the reaction pathway can proceed in two possible directions, i.e., a) continuation of the reaction with the hydrogen radical ($\cdot H$) leads to the formation of the final product methane (CH_4)—the formaldehyde pathway and b) in reaction with the hydroxyl radical ($\cdot OH$) leading to the formation of the final product methanol (CH_3OH)—the carbene pathway [57].

The various representative photocatalytic systems for CO_2 reduction to C_1 products, such as CO, methane, and methanol, and using different types of photocatalysts, reducing agents, and reaction conditions, are summarized in Tables 2–4. All references listed in the tables are discussed in detail in the section related to the corresponding semiconductor. The discussion includes the setup of the experiment for the photocatalytic reduction of CO_2 as well as the obtained results. It is important to emphasize that there is great interest in the formation of C_{2+} products because of their wider use and high added value, as mentioned previously. However, there is a scarce number of papers in the literature related to the reduction of CO_2 to C_{2+} products (such as ethane, ethylene, propane, propylene, ethanol, acetic acid, acetaldehyde, methyl formate, etc.). This can be explained by problems related to the product selectivity towards C_{2+} hydrocarbons. Readers interested in this topic can

find more information in excellent reviews, with an emphasis on describing the current state of the art and the reported photocatalysts to form C_{2+} products, either using H2O or H2 as a reducing agent [39,58].

Table 2. Photocatalytic systems for CO2 reduction to CO.

Photocatalyst	Pressure and Temperature	Reactants	Light Source	CO	Reactor Type/Catalyst Form	References
TNF (0, 240, 40)	1 bar He 0.12 bar CO_2	$CO_{2(g)}$, H_2O	450 W Xe arc lamp	228.3 $\mu mol/g/h$	Stainless-steel A glass microfiber filter impregnated with the solid catalyst	[59]
Cu-TNF (0.5, 240,60)				319.62 $\mu mol/g/h$		
GCN	Ambient pressure, temperature kept at 15 °C by cooling water circulation	$CO_{2(g)}$, $H_2O_{(g)}$	300 W Xe arc lamp	1.28 $\mu mol/g/h$	Air-tight static reactor Photocatalyst deposited on a quartzose plate	[60]
GCN-510				4.18 $\mu mol/g/h$		
3D/2D TiO_2/p-g-C_3N_4 (TOCN-100, TOCN-80, TOCN-50, TOCN-20, HCN, HTO)	Reaction temperature kept at 15 °C by cooling water circulation	$CO_{2(g)}$, $H_2O_{(g)}$	Xe lamp with a 420 nm cutoff filter and average light intensity of 210 mW cm^{-2}	0.209 0.974 $\mu mol/g/h$	Airtight reactor with an optical quartz window at the top	[61]
FeP/CN	Ambient pressure, temperature kept at 15 °C by cooling water circulation	$CO_{2(g)}$, $H_2O_{(g)}$	300 W Xe lamp	5.19 $\mu mol/g/h$	Glass reactor	[62]

Table 3. Photocatalytic systems for CO_2 reduction to methane.

Photocatalyst	Pressure and Temperature	Reactants	Light Source	Methane	Reactor Type/Catalyst form	References
TNF (0, 200, 80)	1 bar He 0.12 bar CO_2	$CO_{2(g)}$, H_2O	450 W Xe arc lamp	62 $\mu mol/g/h$	Stainless-steel A glass microfiber filter impregnated with the solid catalyst	[59]
Cu-TNF (0.5, 240,60)				204,6 $\mu mol/g/h$		
TiO_2	Vacuum, 25 °C	CO_2 $_{(g)}$, $H_2O_{(g)}$	300W Xe lamp	4 $\mu mol/g$ 5 h	Vacuum reactor system Catalyst sprinkled on a circular quartz plate	[63]
0.1% Mo-TiO_2				18 $\mu mol/g$ 5 h		
0.3% Mo-TiO_2				49 $\mu mol/g$ 5 h		
0.5% Mo-TiO_2				11 $\mu mol/g$ 5 h		
NiTiAl-LDH	0.5 bar CO_2 40 °C H_2	CH_3CN: H_2O:TEOA (3:1:1) $Ru(bpy)_3Cl_2 \cdot 6H_2O$	Solar simulator equipped with a Xe arc lamp and an AM 1.5G filter	148 $\mu mol/g/h$	Quartz reactor (55 mL) Dispersed catalyst	[64]
In_2O_3	1.0 MPa 40 °C	$CO_{2(g)}$ $H_2O_{(l)}$	300 W Xe lamp	$(CH_4 + CO)$ $mmol \cdot gcat^{-1}$ h^{-1} 1.088	Stainless-steel autoclave reactor (50 mL) Catalyst suspension	[65]
In_2O_3 with 20% Cu				1.485		
In_2O_3 with 50% Cu				1.485		

Table 3. *Cont.*

Photocatalyst	Pressure and Temperature	Reactants	Light Source	Methane	Reactor Type/Catalyst form	References
Pristine g-CN				69 μmolg^{-1}		
5% V$_2$AlC/g-CN	/	CO$_2$, CH$_3$OH	UV (254 nm) 200 W Hg lamp 100 mW cm^{-2}	101 μmolg^{-1}	Fixed bed, stainless chamber integrated with mass flow controllers (MFC) and cooling fans	[66]
10% V$_2$AlC/g-CN				134 μmolg^{-1}		
10% V$_2$AlC/g-CN	/	CO$_2$, CH$_3$OH	Vis (420 nm) 300 W Xenon reflector lamp 100 mW cm^{-2}	53.6 μmolg^{-1}		

Table 4. Photocatalytic systems for CO$_2$ reduction to methanol.

Photocatalyst	Pressure and Temperature	Reactants	Light Source	Methanol	Reactor Type	Reference
Fe$_3$O$_4$@N-C/Cu$_2$O (12 wt% of Cu$_2$O)	ambient conditions (temperature controlled by a thermostatic water bath at 25 $\pm$ 3 °C)	CO$_{2(g)}$, H$_2$O (1.5 mL), DMF (13.5 mL)	5 W Xenon HID lamp	440 μmol g$_{cat}$$^{-1}$ 3 h	Reaction vessel Dispersed catalyst	[67]
Fe$_3$O$_4$@N-C/Cu$_2$O (12 wt% of Cu$_2$O)	ambient conditions	CO$_2$, H$_2$O, acetonitrile	5 W Xenon HID lamp	410 μmol g$_{cat}$$^{-1}$ 3 h	Reaction vessel	[67]
CeO$_2$ pristine ceria sample				0.5 μmol g^{-1} in 1 h		
UT-CeOx ultrasound treated	at room temperature	H$_2$O, NaHCO$_3$, 0.35 M HCl	visible light/ 300 W xenon light	1.8 μmol g^{-1} in 1 h	150 mL quartz reactor	[17]
UT-CeOx				7.2 μmol g^{-1} in 4 h		
TNTA 10 SILAR			visible light xenon lamp 50 mW/cm^2	70.80 nmol/(cm^2·h) 6 h 193.63 nmol/(cm^2·h) 6 h		
	60 °C	CO$_{2(g)}$ (flow rate = 20.5 mL/min) H$_2$O$_{(g)}$		193.63 nmol/(cm^2·h) 6 h	Optofluidic planar microreactor (high 0.04 cm, reaction area 2.5cm x 2cm)	[68]
CdS/ZnS-TNTA 10 SILAR			visible light xenon lamp 110 mW/cm^2	255.49 nmol/(cm^2·h) 6 h		
3.74% N-In$_2$O$_3$	25 °C, 1.01 bar	CO$_{2(g)}$, H$_2$O$_{(l)}$, 10 vol.% TEOA	Xenon lamp (300 W)	394 μmol g$_{cat}$$^{-1}$ h^{-1} 6 h	Gas circulation-evacuation reactor Dispersed photocatalyst	[16]

2.5. Photocatalysts for CO$_2$ Reduction

2.5.1. TiO$_2$-Based Photocatalysts

The highly efficient conversion of CO$_2$ into valuable fuels and chemicals requires a balance between the low band gap of the photocatalyst for enhanced light absorption and a large surface area that can facilitate the adsorption of CO$_2$ molecules on the photocatalytic surface. In addition, the process of charge dynamics must be achieved, i.e., the e-h separation/transfer must be controlled to minimize the fast recombination of the photogenerated charge carriers. Therefore, enormous efforts have been made to develop efficient photocatalytic materials for selective CO$_2$ reduction to desired products, including TiO$_2$-based photocatalysts, various metal oxides, Z-scheme heterostructures, metal–organic frameworks (MOFs) and their composites, carbon nitrides, layered double hydroxides (LDHs), etc. It is important to mention that the comparison of the photocatalytic activity

and selectivity from the published results is very difficult due to the different experimental conditions (i.e., synthesis method, photocatalyst configuration, CO_2 flow rate, type and content of reductant, presence of sacrificial electron donors and/or co-solvents, irradiation and illumination intensity, and reaction conditions such as temperature and pressure) and the photoreactor geometry used.

Titanium dioxide (TiO_2) is considered one of the most efficient and environmentally benign photocatalysts and is widely used for CO_2 reduction and photodegradation of various pollutants. Recently, titania in the form of 1D materials as titania nanotubes (TNTs) with a diameter of 10–100 nm and a length of 1 µm has attracted even more attention due to their unique physicochemical properties [63,64]. Ti-based photocatalysts (Ti-based zeolites and Ti-based MOFs) for CO_2 photoreduction have been reviewed by Li et al. [69]. They show some tailoring strategies such as heterojunction construction, cocatalyst modification, element doping, and surface adjustment that can improve the photocatalytic activity.

Camarillo et al. [59], synthesized titania nanofibers (TNFs) from titanium isopropoxide (TTIP) precursor at different pressures (200–240 bar) under supercritical CO_2 atmosphere and temperatures (40–80 °C). Ten different materials were prepared, six of which are TiO_2 nanofibers marked as TNF (0, 200, 40), where the first number in the bracket indicates the Cu weight fraction, the second the pressure (bar), and the third the temperature (°C), and four other TiO_2 doped with Cu at different concentrations marked as (Cu-TNF). The presence of Cu slightly increased the BET surface area up to 262 m^2g^{-1} for Cu-TNF (2, 240, 60). The photocatalytic activity of the prepared materials was tested in a 50 mL reactor (stainless-steel chamber) equipped with a Xe arc lamp (Oriel, 450 W) and an Air Mass 1.5 Global filter (irradiance 100 mW cm^{-2}), valves for gas feeding, evacuation, and connection to a Micro-GC (Agilent) system, a CO_2 flow controller, and a bubbler containing deionized water to moisten the gas (CO_2 + He) before entering the reaction chamber. The glass microfiber filter uniformly impregnated with the solid catalyst (40 ± 5 mg) is placed in the reaction chamber and under He condition at 1 bar was achieved at a -10 °C dew point to dry the installation. Then, the dew point was increased to 20 °C passing in wet helium to prevent the condensation of water vapour. The reactor was then filled with CO_2 to a differential pressure of 0.12 bar and the photocatalytic reaction was started by switching on the Xenon lamp. The main products were CO and CH_4 but with a higher production rate of CO. The reason for the higher production rate of CO (228.3-319.6 µmol/g/h) than for CH_4 (62–204.6 µmol/g/h) might be that the formation of methane requires eight electrons, while CO requires only two electrons [70]. They show that undoped and Cu-doped TNFs have higher CO_2 reduction rates (200 to 250 µmol/g/h) than commercial catalysts (P-25), with the formation rate of CO around 200 µmol/g/h and those of CH_4 ranging from 25 to 75 µmol/g/h. In particular, the catalyst with a higher methane production rate (62 µmol/g/h) was TNF (0, 200, 80). It was also found that a catalyst doped with 0.5 wt.% Cu produced 3.3 times more methane and 1.4 times more CO than a corresponding undoped catalyst. The catalyst with the highest total production rate among all synthesized ones was also the catalyst doped with 0.5 wt.% Cu (1.7 times higher than the undoped catalyst). Cu-TiO_2 catalysts exhibit high photocatalytic activity because Cu particles act as electron acceptors. In this context, higher Cu content decreases the surface area of TiO_2 and the photoexcitation ability. Thus, Cu-TNF (0.5, 240, 60) gave better results than Cu-TNF (2, 240, 60) and Cu-TNF (1, 240, 60).

Another approach to modifying the one-dimensional nanotube arrays of TiO_2 (TNTA) was its modification with the semiconductors of different band gaps such as CdS (E_g = 2.4 eV) and highly reductive ZnS (E_g = 3.7 eV). The SILAR method (successive ionic layer adsorption and reaction cycles) was used to deposit CdS/ZnS composite catalysts as quantum dots (QDs) on TNTA. A few nanocomposites of CdS/ZnS-TNTA with different amounts of CdS/ZnS (QDs) were prepared for 0, 4, 7, 10, 13, and 16 SILAR cycles [68]. The advantages of this modification of TiO_2 with CdS/ZnS are the response to visible light with highly negative CB and the strong reducibility. In addition, due to the relatively small wall thickness of 1D TNTA, the diffusion distance of the photogenerated charge carriers is short-

ened, so the recombination rate of the photocarriers is low. In addition, TNTA has a high specific surface area and adsorption capacity. The photocatalytic activity of the prepared CdS/ZnS-TNTA nanocomposites was studied in a planar microreactor (high 0.04 cm, reaction area 2.5 cm × 2 cm) filled with gaseous CO_2 (volume flow rate = 20.5 mL/min) and water vapour as reactants at 60 °C for 6 h. The sunlight was simulated with a xenon lamp placed above the microreactor. The main product of the reduced CO_2 was methanol. The yield of methanol product with CdS/ZnS-TNTA at a visible-light intensity of 50 mW/cm^2 was 193.63 nmol/(cm^2·h) and was almost three times that of unmodified TNTA (70.80 nmol/(cm^2·h)) when TNTA was treated with 10 SILAR cycles. The highest product yield of 255.49 nmol/(cm^2·h) was achieved with the illumination intensity of 110 mW/cm^2 and is attributed to the increase in light intensity and sensitization with CdS/ZnS QDs, which broadened the absorption in the visible spectrum and prevented the recombination of electron-hole pairs. They also investigated the influence of different flow rates of CO_2 (4.5–30 mL/min) on the photocatalytic reduction of CO_2. They show that as the CO_2 flow rate increases, the methanol yield also increases up to the optimal flow rate (20.5 mL/min), after which the product yield begins to decrease. This can be explained by the fact that the product yield is initially low at a low CO_2 flow rate because the reactant takes longer to diffuse to the surface of the photocatalyst and because it takes longer for the reactant to be renewed during the reaction. Furthermore, increasing the CO_2 flow rate accelerates the arrival of reactants at the surface of the photocatalyst, but also the desorption of the products, preventing the reoxidation process.

Sanz-Marco et al. [71], synthesized Ni/TiO$_2$ by photo-assisted deposition of Ni salts under LED irradiation at 365 nm onto TiO$_2$ P25 nanoparticles in CH$_3$OH as a hole scavenger. In this way, the surface of TiO$_2$ is coated with a 2 nm thick layer and approximately 2 mass% of Ni particles. The as-prepared material is subjected to thermal reduction at 400 °C under 10% H$_2$ to produce TiO$_{2-x}$ oxygen defects. The photocatalytic activity of the material prepared in this way (120 mg) was tested for the reduction of CO_2 to the final products CO, CH$_4$, and C$_2$H$_6$ in a fixed-bed prismatic quartz reactor at 365 nm, 460 nm, and white light (LED source). Before the photocatalytic reaction, the deaeration of the reactor was done for 30 min, introducing a gas mixture of CO_2 and H$_2$ (1:4 molar ratios). Then, the photocatalytic reaction of the CO_2 + H$_2$ gas mixture (1.7 bar, 250 °C) was started by switching on the LED. At 365 nm, the Ni/TiO$_2$ (without pretreatment) catalysts produced 450 µmol g$_{cat}^{-1}$h^{-1} methane and 250 µmol g$_{cat}^{-1}$h^{-1} of CO. The catalyst activation by H$_2$ treatment at the high temperature significantly increased the photocatalytic activity under UV light, and the catalytic response is extended to the visible region of the solar spectrum. The formation of both bulk and surface-oxygen vacancies on the TiO$_2$ could explain the higher production of CO and C$_2$H$_6$ (about 4 µmol g$_{cat}^{-1}$h^{-1}) under UV light for the Ni/TiO$_2$-A. Oxygen vacancies might act as electron traps, facilitating charge-carrier separation and charge transfer to the adsorbed species. Under UV LED irradiation, the formation of methane was less effective at ~400 µmol g$_{cat}^{-1}$h^{-1}. The Ni/TiO$_2$-A catalyst produced around 75 µmol g$_{cat}^{-1}$h^{-1} under LED illumination at blue light (460 nm) while it produced less than 50 µmol g$_{cat}^{-1}$h^{-1} under white LED.

A wide variety of noble metal cocatalysts have been tested for the hydrogenation of CO_2 into alkanes in the gas phase mediated by Sabatier's reaction e. The noble metals as cocatalysts could increase the CH$_4$ product selectivity in photocatalytic CO_2 reduction by TiO$_2$. However, due to their price and a limited amount in nature, cheaper alternatives are needed. Feng et al. [63] performed the photoreduction reaction of CO_2(g) with water in the gaseous phase in a vacuum reactor connected to a cooling system. The whole process took place at 25 °C, and a Xe-lamp was used as a light source. TiO$_2$ or Mo-doped TiO$_2$ powder was sprinkled on a circular quartz plate with a diameter of 50 mm. They proposed that Mo-doped TiO$_2$ with increasing Mo concentrations (0.3 wt%) increased the photocatalytic conversion of CO_2 and selectivity up to 54.1% towards methane formation. The present results indicate that photocatalytic CO_2 reduction over TiO$_2$-based catalysts may follow the fast-deoxygenation pathway. After the fifth hour of irradiation, the mean CH$_4$ yields

were 4, 18, 49, and 11 μmol/g for TiO_2, 0.1% Mo/TiO_2, 0.3% Mo/TiO_2, and 0.5% Mo/TiO_2, respectively. Here it is evident that, with further increasing of the Mo concentrations, the CH_4 selectivity begins to decrease.

2.5.2. Indium Oxide

Indium oxide (In_2O_3) is an n-type of semiconductor with a narrow band gap (~2.8 eV) exhibiting good stability, high activity, and photo corrosion resistance. The pristine In_2O_3 can be activated only under UV irradiation and has a low activity for photocatalytic reduction of CO_2 due to the fast recombination of the photogenerated electrons and holes. By changing the surface properties and crystal structure of the pristine pale-yellow In_2O_3 into In_2O_{3-x}, it becomes black and extends into the visible-light region.

Recently, Yang et al. [16] have synthesized a nitrogen-doped indium oxide (N-In_2O_3) photocatalyst via dielectric barrier discharge (DBD) plasma. The photocatalytic reduction of CO_2 with water was carried out in a closed gas circulation-evacuation reactor in the presence of 0.1 g of the photocatalyst dispersed in 100 mL of 10 vol.% triethanolamine (TEOA) at ambient conditions (25 °C, 1.01 bar) for 6 h. The xenon lamp (300 W) was used as a light source. TEOA was used as a sacrificial agent to capture photogenerated holes, thus releasing more photogenerated electrons for reducing CO_2 with water. The two main products were methanol and CO. At a nitrogen content of 3.74%, the highest methanol formation rate of 394 μmol g_{cat}^{-1} h^{-1} and a selectivity of 63% were achieved. The prepared photocatalyst showed high stability after five runs. They also showed that nitrogen doping generates midgap energy states and reduces the band gap of In_2O_3, enhancing photon absorption and electron-hole separation. Moreover, nitrogen doping creates more oxygen vacancies on In_2O_3, leading to more active sites for CO_2 adsorption and conversion [16].

Copper (Cu)-decorated indium oxide (In_2O_3) rods were prepared by a simple wet-chemistry method under ambient conditions and tested in photocatalytic CO_2 conversion under simulated sunlight [65]. Photocatalytic CO_2 reduction was carried out in a stainless-steel autoclave reactor (50 mL) filled with 1.0 MPa CO_2, at 40 °C and under irradiation at 300–500 nm with an intensity of 300 mW cm^{-1} for two hours. The light source was a 300 W Xe lamp, Pls-sxe 300+. For this photocatalytic reaction, the catalyst was used in a water suspension of 1gL^{-1}. Interestingly, the high total evolution rate of (CH_4 + CO) was 1.088 mmol·gcat^{-1} h^{-1} by using pristine In_2O_3 without Cu incorporation. The simultaneous formation of H_2 indicates the presence of competing reactions for CO_2 conversion, but the selectivity to the desired products was high, 88.8%. With the addition of 20% Cu, the total evolution for carbon-based products (CH_4 + CO) increased by 36.5% compared to the pristine In_2O_3, reaching 1.485 mmol gcat^{-1} h^{-1}. The total carbon evolution reached 4.985 mmol g_{cat}^{-1} h^{-1} by further increasing the Cu loading to 50% (Cu0.5In0.5). This represents an increase of 358% compared to the pristine In_2O_3 (Cu0In1). However, only 17.3% of hydrogen was produced in the total products when 50% Cu was incorporated into the sample. In this work, the formation of hydrogen is not explained, but there is concern that a water-splitting reaction occurs simultaneously [65]. Although the authors of this paper believe that such a high yield of products (mmol) is promising for future industrial applications, we propose to re-evaluate the photocatalytic activity of the prepared photocatalysts under the same reaction conditions.

2.5.3. Cerium Oxide

Recently, cerium oxide (CeO_2) has drawn attention as a photocatalyst due to its nontoxicity, distinctive structure, and simple oxidizing capabilities. The major drawback of its application in photocatalytic CO_2 conversion with solar energy is the wide energy band gap [26].

The cerium oxide nanostructure can be synthesized under ultrasound irradiation in an alkaline medium by the sol-gel method for rich surface defects [17]. The ultrasonic treatment of the cerium oxide nanostructures leads to the formation of surface-oxygen vacancies which increase the efficiency and selectivity of photocatalytic CO_2 reduction to

methanol over CO. The photocatalytic activity of the synthesized samples was examined by CO_2 reduction. The reaction was carried out in a 150 mL quartz reactor under visible light using a 300 W xenon lamp at room temperature. In this study, the pristine ceria sample produced both CH_3OH (0.5 µmol g^{-1}) and CO (0.15 µmol g^{-1}) in one hour, while the ultrasound-treated CeOx sample resulted in enhanced and selective production of CH_3OH (1.8 µmol g^{-1}) along with CO (0.054 µmol g^{-1}). After 4 h of irradiation, the production of CH_3OH was 7.2 and 2 µmol g^{-1} for the UT-CeOx and CeO_2 samples, respectively. The final products exhibited excellent stability, and the smaller particle size increased the photocatalyst surface area and charge-carriers separation efficiency [17].

Zeng et al. [72] prepared PCN-RuCu photocatalysts for the selective conversion of CO_2 to valuable fuel by the simultaneous incorporation of ruthenium and copper single atoms into polymeric carbon nitride (PCN). The results have shown that the PCN-RuCu sample exhibited much higher selectivity (95%) for CH_4 production than the individual Ru- or Cu-decorated PCN during photocatalytic CO_2 reduction under visible-light irradiation. It was revealed by DFT calculations that the coexistence of Ru-N_4 sites and Cu-N_3 sites can effectively tune the electronic structure of PCN, making the Ru sites account for photogenerated electron-hole pairs and the Cu sites for CO_2 hydrogenation. Moreover, the synergistic effect between Ru and Cu single atoms significantly promotes the consecutive hydrogenation processes of *CO species for CH_4 production.

2.5.4. Z-Scheme Heterostructures

The design of the Z-scheme heterostructure is an attractive strategy for efficient charge separation at the interface to promote photocatalytic CO_2 reduction. Wang, et al. [15] prepared a $BiVO_4/Bi_2S_3$ composite through an in situ selective epitaxial growth of Bi_2S_3 nanosheets on the facets of $BiVO_4$. They discovered by X-ray photoelectron spectroscopy that the delocalized electrons in the Bi_2S_3 nanosheets transfer to the $BiVO_4$ within the $BiVO_4/Bi_2S_3$ heterostructure, and an internal electric field (IEF) generated at the interfaces drives the photoinduced electrons in $BiVO_4$ to Bi_2S_3 under light irradiation, resulting in a direct $BiVO_4/Bi_2S_3$ Z-scheme heterojunction. Moreover, they prepared unique $MnO_x/BiVO_4/Bi_2S_3$ heterostructures by photodepositing the MnOx cocatalyst onto the facet of $BiVO_4$ for CO_2 conversion. They showed that the $MnO_x/BiVO_4/Bi_2S_3$ heterostructure facilitated the photocatalytic reaction by transferring the photogenerated electrons and holes to the Bi_2S_3 and MnO_x surfaces, thereby catalyzing the CO_2 photoreduction into methanol and water oxidation with stoichiometric oxygen formation in the absence of a sacrificial agent, respectively [15].

Conversion of CO_2 by photoreduction into CH_4 and CO, with yields of 37.4 and 21.7 µmol g^{-1} h^{-1}, respectively, was achieved with (Au/A-TiO_2)@g-C_3N_4 Z-scheme heterojunction [73].

2.5.5. MOF-Based Composites

To diminish the energy shortage, the current challenge is to develop metal–organic framework materials (MOFs). The semiconducting nature of highly porous MOFs increases their application potential for the production of enhanced energy fuels. MOFs are composed of metal nodes and organic linkers. Metal–organic frameworks are crystalline materials with unique properties, such as a large surface area, high content of transition metals, and the possibility of being designed and modified after synthesis.

MOFs are characterized by their unique structural properties, tunable pore environment, and large surface area. MOFs and their composites can be used for the production of hydrogen, methane, ethanol, methanol, acetic acid, and carbon monoxide as renewable fuel energy sources [74]. These unique properties have drawn the attention of researchers to their applications in photocatalysis and photothermal catalysis. MOF-based photocatalysts have finely engineered band gaps and catalytic active sites, as well as efficient charge-transfer pathways due to the high number of metal nodes and organic linkers [75]. The active sites may be coordinatively unsaturated metal ions, substituents on the organic

linkers, or guest species located inside the pores. The higher catalytic activity of MOFs compared to other solid materials is due to the activation of the substrate at more than one site or the simultaneous activation of different substrates by complementary active sites on the MOF. The structure of MOFs allows the adaptation of linkers as light absorbers and the exchange of metals in MOF nodes to improve photoinduced electron transfer and optimize their photocatalytic activity using visible light, which explains the current interest in using these materials for the photocatalytic reduction of CO_2 [76].

Graphitic carbon nitride quantum dots (g-CNQDs) coupled to Zr (IV)-based MOF (g-CNQDs@MOF) have been prepared as MOF-based composites for the selective photoreduction of CO_2 to methanol under visible-light irradiation [77]. g-CNQDs enhanced the electronic conductance properties of the MOF composite by increasing the lifetime of the photogenerated electron-hole pairs on the surface. Zhan et al. [78] reviewed and discussed the various modification strategies for the development of efficient MOF-based photocatalysts, which can promote the understanding of the relationship between structure and catalytic performance. MOF-based photocatalysts can be classified as pure MOF materials, MOF composites, and MOF derivatives. MOF composites consist of MOF materials and foreign functional materials, such as metal nanoparticles (NPs), semiconductors, and carbon materials. Various MOF materials have been reported as efficient photocatalysts for the reduction of CO_2 [78]. They explained the mechanism of activation of MOF semiconductors, which includes the formation of LUMO and HOMO, i.e., the formation of electrons and holes in the CB and VB after irradiation with energy equal to or higher than the band gap of the MOF semiconductor. Then, the photogenerated electrons can be transferred to the active sites through the possible mechanisms of linker-to-metal charge transfer (LMCT) [79], metal-to-metal charge transfer (MMCT) [80], and linker-to-linker charge transfer (LLCT) [81], since both the metal nodes and linkers in MOFs can act as active sites for the photocatalytic CO_2-reduction reaction (CO_2RR). Finally, the photogenerated electrons with sufficient energy undergo the reduction reaction with CO_2. Meanwhile, the holes generated by light react with the electron donors to complete the whole process.

Xiao et al. [82] have shown that MOFs can be used to influence the shift in the activation wavelength of the photocatalyst and thus the energy required for the creation of electron-hole pairs, as well as redox reactions at the surface. In addition, MOFs are also used in photothermal catalysis when combined with plasmonic metals [82].

2.5.6. Carbon Nitrides

Carbon nitride (CN)-based materials have many advantages over conventional inorganic metal-based semiconductor photocatalysts, including simple and inexpensive fabrication, high physicochemical and thermal stability, and recyclability without leaching toxic metals through photo corrosion (since they are metal-free). Due to their suitable band gap (2.7 e V) and their ability to absorb visible light, CNs are promising catalysts for CO_2 photoreduction, and are therefore being studied by many researchers. Unfortunately, extended light absorption does not always signify enhance photocatalytic performance due to the insufficient adsorption/activation of the reactants over the low specific surface area and the high recombination rate of the photogenerated e^-/h^+ pairs [60–62]. Therefore, research in this field is primarily focused on advancement in the synthesis of nanostructured and functionalized CN-based hybrid materials. Some examples of recent research are described below, including the implementation of novel functionalized nanostructured CNs and their hybrid heterostructures. The activation of CO_2 to CO using CN-based materials has been demonstrated several times by Zhang et al., who used, besides others, carbon-vacancy modified graphitic carbon nitride (GCN510) [60], two-dimensional porous graphite-like carbon nitride nanosheets decorated with three-dimensional hierarchical TiO_2 microflowers (3D/2D TiO_2/p-g-C_3N_4) [61], and heterostructured iron phosphide-modified polymeric carbon nitride (FeP/CN) [62]. According to their investigation, the introduction of carbon vacancies in GCN enhances the CO_2 conversion into CO, with a CO evolution rate of 4.18 μmol g_{cat}^{-1} h, which is 2.3 times higher than that of pristine GCN. The improved CO_2

reduction performance is attributed to the enhanced CO_2 adsorption/activation, upshifted conduction band, and elevated charge-carrier concentration and lifetime. On the other hand, the excellent adsorption and photocatalytic properties of multifunctional 3D/2D TiO_2/p-g-C_3N_4, prepared through a one-pot hydrothermal method, are mainly attributed to the enlarged surface areas and pore volumes, increased adsorption/active sites, improved light absortion and enhanced charge separation efficiency based on interfacial heterojunctions and surface carbon vacancies. In another interesting paper, promising results were reported dealing with a heterostructured composite FeP/CN catalyst prepared by the gas-phase phosphorization of FeOx/CN precursor. In this reaction system, the optimized FeP/CN (0.15, 400) photocatalyst exhibited the highest CO evolution rate of 5.19, which is 5.5 times the rate for pure CN (0.95). The enhancement of photoactivity is explained as follows: (i) the enhanced light absorption of FeP/CN in the visible and UV regions due to the introduction of FeP, (ii) the reduced charge-transfer resistance, and (iii) the promotion of the formation of the *HCOO intermediate during CO_2 photoreduction by the incorporation of FeP [62].

Single Co^{2+} sites which exist in the $Co-N_{2+2}$ coordination at the edges of C_3N_4 flakes in graphitic carbon nitride (C_3N_4) have also demonstrated excellent activity and selectivity in photocatalytic CO_2 reduction. Carbon doping of C_3N_4 is found to be important for the photocatalytic properties of the single Co^{2+} sites. The presence of a C dopant near the metal centres results in a shorter Co–N bond length and stronger Co-N binding energy. In addition to the enhanced light absorption and charge separation in C-doped C_3N_4, the stronger Co-N binding upon C doping likely contributes to the improved catalytic properties of the single Co^{2+} sites [83].

Xia et al. [84] prepared the crystalline carbon nitride with a surface-defect design to enable the effective gas-phase CO_2 photoreduction into hydrocarbon fuels while oxidizing water to oxygen. In a typical photocatalytic experiment, they put 100 mg of the photocatalyst onto the bottom of a two-neck Pyrex reactor with two parallel planes in 41% humidity and a 350 W Xe lamp with an AM1.5 filter was used as a light source. Then, 0.084 g of $NaHCO_3$ was added. Deaeration of the reactor has done by N_2 for 1 h. Then, the reaction between 0.3 mL of 2 M H_2SO_4 and $NaHCO_3$ leads to the formation of CO_2 in the sealed reactor. Under irradiation, the photocatalytic CO_2 conversion generates methane, methanol, and ethane, as well as carbon monoxide and oxygen. At 86% humidity, the total production yield and selectivity of hydrocarbons over carbon nitride crystals (CCN) are 12.07 $\mu mol\ h^{-1}\ g^{-1}$ and a selectivity of 91.5%, both values significantly higher than those of most previous carbon nitride photocatalysts. The total production yield of (CH_4, CH_3OH, and C_2H_5OH) is 5.82 $\mu mol\ h^{-1}\ g^{-1}$. The polymeric carbon nitrides were synthesized by co-condensation of guanidine hydrochloride and dicyandiamide under acetonitrile-promoted solvothermal conditions, with good selectivity for hydrocarbons in the absence of any cocatalyst or sacrificial agent [84].

Tahir et al. [66] prepared a nanocomposite of vanadium aluminium carbide (V_2AlC) MAX coupled with porous graphitic carbon nitride (g-CN) for photocatalytic CO_2 reduction. The 2D/2D V_2AlC/g-CN performance was conducted in a fixed-bed and monolith photoreactor under UV and visible light. The V_2AlC/g-CN exhibited photoactivity of 67 $\mu mol\ g^{-1}\ h^{-1}$ for CH_4 evolution, which was 1.94 fold more than their production compared to using pristine g-CN. More importantly, the highest productivity was obtained with the CO_2-CH_3OH sacrificial reagent because methanol attaches more strongly to g-C_3N_4 and produces more protons. The performance of V_2AlC/g-CN under UV light was also promising due to the ability of long pathways to penetrate light inside the fixed-bed reactor. The monolith photoreactor (2×6 cm with 200 channels per square inch) has higher productivity for CO_2 reduction to CH_4 due to the large illuminated active surface area, better light utilization, and efficient mass transfer within the monolithic microchannels. In a typical experiment, 150 mg of the photocatalyst was cleaned with He gas for 30 min before use. They found that a certain amount of V_2AlC MAX as a cocatalyst (up to 10%) increased the formation of methane due to the separation of photo-induced charge carriers,

while the higher loading resulted in lower methane production due to a lower surface area for the photocatalytic reaction. They also found that the 10 V_2AlC/g-CN nanocomposite resulted in 2.5 fold higher methane formation under UV irradiation with the mercury lamp (200 W) at 254 nm than under visible light produced with the xenon lamp (300 W) at about 420 nm. Both lamps have the same intensity of 100 mW cm^{-2}. Obviously, the light source significantly influences the formation of the product under the same experimental conditions, which was explained by the deeper penetration of UV than visible light and the higher production of charges. The other reason could be the long travelling distance of light (8 cm length) before the photoactivation process.

Movahed et al. [67], developed copper oxide (I) nanoparticles decorated on nitrogen-doped carbon (*N*-C) in the form of a rod-shaped core-shell nanostructure. The photocatalytic activity of the rod-shaped core-shell nanostructure Fe_3O_4@*N*-C/Cu_2O was used for selective CO_2 reduction into methanol. It was found that the developed nanohybrid structure exhibited about four-times higher activity than the Fe_3O_4@Cu_2O photocatalyst, which could be due to the enhancement of visible-light absorption and the facilitation of separation of photogenerated electron-hole pairs [67]. The photocatalytic reduction experiments were performed in a reaction vessel equipped with a 5 W xenon HID lamp with an irradiance of 12.5 mW cm^{-2} under ambient conditions in a DMF–water mixture as a solvent. After 3 h of visible-light illumination in the presence of nanohybrids, methanol was produced as the major product of CO_2 photoreduction. The results showed that the highest yield of methanol was 440 μmol $g_{cat}$$^{-1}$ when 12 wt% Cu_2O was supported on the Fe_3O_4@*N*-C. The aggregation of Cu_2O nanoparticles occurred with a further increase in the amount of copper oxide in the Fe_3O_4@N-C/Cu_2Oc, resulting in an increase in the charge-recombination centres for the photogenerated electron-hole pairs. The experimental results showed that Cu_2O plays a key role in CO_2 photoreduction since Fe_3O_4@N-C has low photocatalytic activity. The photocatalytic activity of Fe_3O_4@N-C/Cu_2O for CO_2 reduction was about four-times higher than that of the Fe_3O_4/Cu_2O photocatalyst, which might be due to the enhancement of visible-light absorption and the facilitation of separation of photogenerated electron-hole pairs. They also performed the experiment in a polar aprotic solvent (acetonitrile) to prove that the formation of methanol was due to the photocatalytic reduction of CO_2 and not DMF. They found a similar concentration of the methanol product in acetonitrile as in DMF, namely 410 μmol $g_{cat}$$^{-1}$. Moreover, no formation of methanol was observed in the reaction with DMF and photocatalyst in the absence of CO_2, confirming methanol generation by CO_2 photoreduction.

2.5.7. Layered Double Hydroxides

Layered double hydroxides (LDHs) are an emerging family of materials with interesting photocatalytic properties that are gradually being used for CO_2 photoreduction to useful chemicals [64]. A new NiTiAl-LDH material was prepared by a modified solvothermal process containing Ni, Ti, and Al within the structure to increase the selectivity for methane production [64]. The material was tested in a closed quartz reactor (55 mL volume) under solar simulator conditions and resulted in a methane production of 148 μmol g^{-1} h^{-1} with a selectivity of 86%, while competition from hydrogen evolution was almost suppressed. For the photocatalytic reaction, 20 mg of the catalyst was dispersed in 20 mL of acetonitrile (CH_3CN): water (H_2O): triethanolamine (TEOA) = 3:1:1. After 15 min of sonication, 6.6 mg of Ru(bpy)$_3Cl_2$·6H_2O were dissolved in this suspension. After 15 min of stirring, the final overpressure of pure CO_2 in the photoreactor was 0.5 bar and the temperature of the reactor was maintained at 40 °C during the experiment. The irradiation was carried out with a Newport Oriel® Sol1A™ Class ABB 94041A solar simulator equipped with a Xe arc lamp and an AM 1.5G filter.

The role of Ti in selectivity toward methane was confirmed as no CH_4 was produced when a NiAl-LDH catalyst was used instead. No catalytic activity was observed in the absence of TEOA or Ru(bpy)$_3Cl_2$. In the case of NiAl-LDH, the main product was CO and some hydrogen, while methane was not. This selectivity was attributed to the band

structure of the Ti-containing material, whose band edge placement is more suitable for CO_2 reduction to CH_4 than CO. The electronic interaction between Ni(II) and Ti(IV) causes a shift in the band-edges position and reduces the optical band gap of the material.

The LDH has a laminar structure with two positively charged host layers of $M(OH)_6$ (M = Cu, Co, and Al) octahedral and an interlayer occupied with charge-balancing CO_3^{2-} anions. Due to the strong interaction between CO_2 and hydroxyl groups on the LDH, gaseous CO_2 can be easily captured and stored as interlayer CO_3^{2-} which is stabilized by the electrostatic force between the host layers and the CO_3^{2-}. The interlayer CO_3^{2-} is directly involved in photoreduction instead of CO_2, which is confirmed by the generation of CO under illumination in a CO_2-free atmosphere [85].

2.6. Choice of Photocatalytic Supports

The design of fixed-bed reactors for CO_2 photoreduction, in both the liquid and gas phase applications, is influenced by the choice of photocatalytic supports, since the interaction between the anchored photocatalyst, reactants, and light must be optimized. Due to the adjustable geometric surface (number and dimensions of channels), increasing emphasis is being placed on monolithic rather than suspension and ring reactors. Ceramic, plastic, and metal materials are used to make monolithic substrates (uniform parallel channels) on which the catalyst is deposited in the form of a film in or on the surface. Before coating the active catalytic material, the monoliths are usually precoated with an inorganic oxide to ensure a good bond between the monolith and the catalyst.

The main drawbacks of catalysts immobilized on monolithic multichannel substrates include limited accessibility of the catalytic surface to photons and reactants and reduced active sites of the catalysts due to insufficient light penetration. Limited accessibility of the catalytic surface to photons and reactants and reduced active sites of the catalyst due to insufficient light penetration are the main drawbacks associated with catalysts immobilized on monolithic multichannel substrates [86].

3. Photoreactor Design and Configuration

In addition to the development and selection of suitable semiconductor material with high quantum yield, the design and optimization of the photocatalytic reactor also have a decisive influence on the photocatalytic efficiency. The basic function of photoreactors is to provide good contact between the illuminated catalyst and the reactants [87,88]. Although considerable efforts have already been made in the development of photocatalysts, little attention has been paid to the design of photoreactors [19].

The key factors affecting the efficiency of the CO_2 photoreduction system are the number of phases present (mainly a multiphase system, i.e., gas–solid, liquid–solid and gas–liquid–solid), the mode of operation (batch, semibatch, and continuous or flow type), the design of the photocatalyst, i.e., its placement inside the photoreactor (suspended vs. supported or immobilized photocatalyst), and the choice of reducing agent. This results in a large number of different designs of photoreactors [19,45,89–96]. Other parameters that influence the operation of the photoreactor are the irradiation source, the design of the reactor in terms of the position of the irradiation source (inside or outside the reactor), the material that the reactor is made of (stainless steel, Pyrex, quartz, etc.), the heat exchange and mixing, or the type of contact between the phases.

The simplest version refers to a suspension photoreactor and common semiconductor photocatalysts. In the photoreactors with an impregnated photocatalyst layer, the photocatalytic material can be immobilized on the walls of the reactor or deposited on suitable supports (glass plates, filters made of glass fibres, stainless-steel mesh, glass wool, optical fibres, monoliths, etc.), and such an immobilized layer can be placed at different locations of the photoreactor (at the bottom, in the middle, under a certain inclination, etc.). The porous structure and the large specific surface area of the support can lead to better adsorption of CO_2 and, consequently, to higher conversion into the expected products due to the presence of more active sites on the photocatalyst. The most important parameters in the

design of such a porous system are the choice of the optimal thickness of the photocatalytic layer and the position of the immobilized photocatalytic layer and/or photoreactor in relation to the irradiation source. For photoreactors with an immobilized photocatalyst, the resistance to mass transfer determines the overall efficiency of the system. In this case, appropriate engineering solutions are applied to minimize the resistance to mass transfer. This can be achieved by choosing process parameters such as partial pressure, temperature, mixing/turbulence, the specific surface area of the photocatalyst, pH, and the performance of the photoreactor itself. Ceramic monolithic supports of catalytically active components stand out from the usual photocatalytic-layer supports. However, their production is very demanding and is usually carried out with specially designed equipment (extruders). Recently, significant progress has been made in this regard, due to the application of additive technology (or 3D printing), which is still in its infancy in the preparation of heterogeneous (photo)catalysts.

Depending on the design/form of the photocatalyst, photoreactors are divided into slurry photoreactors, fixed-bed photoreactors, and membrane photoreactors (Figure 6). A detailed discussion of all the above reactors can be found in the literature [19,45].
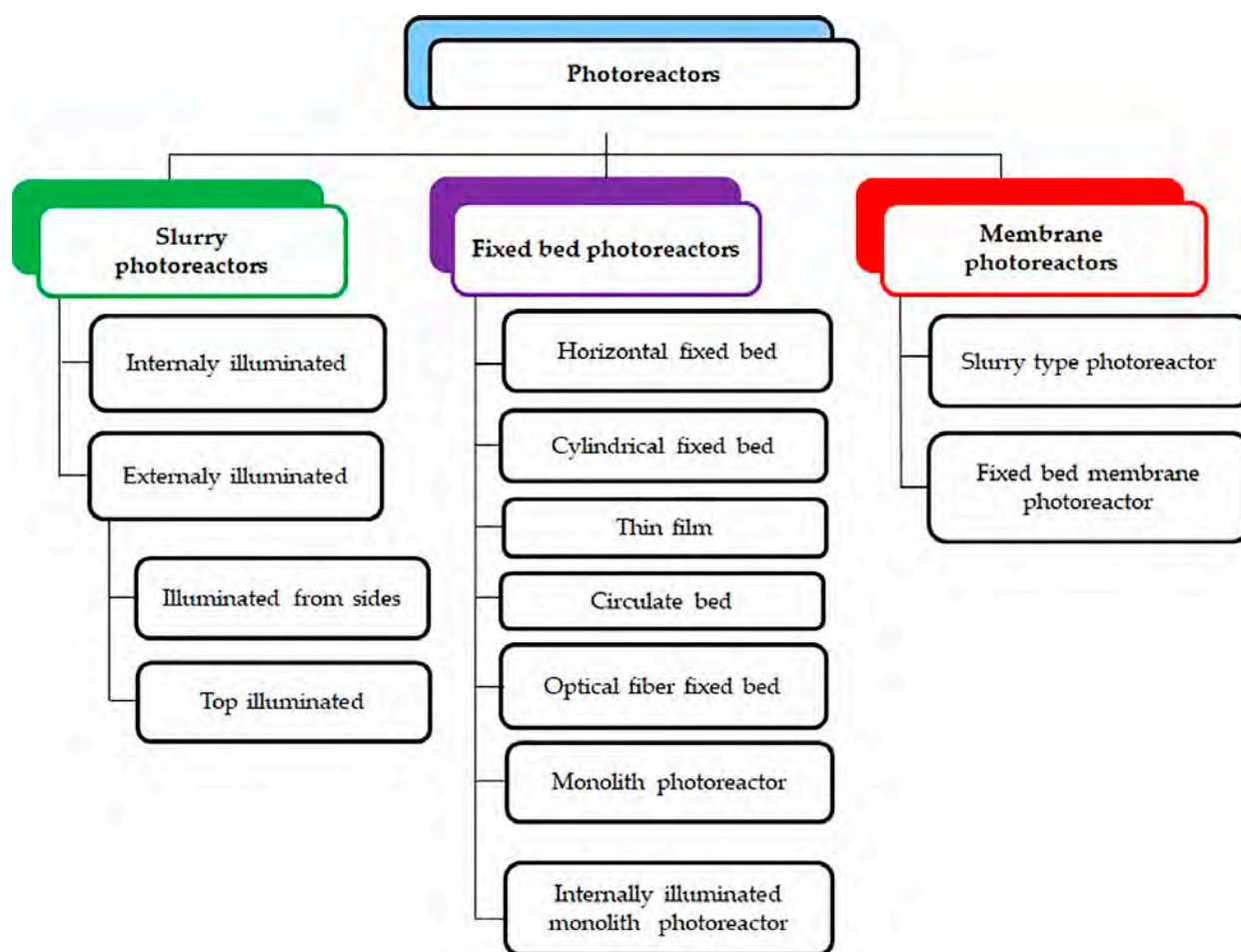

Figure 6. Possible classification of the photoreactor design used for CO_2 photoreduction.

3.1. Slurry Photoreactors

Suspension photoreactors are most commonly used in practice and refer to multiphase systems in which CO_2 is in the gaseous phase, the reducing agent is usually in the liquid phase, and the catalyst is dispersed/suspended in a liquid medium. The reductant is usually water with or without additional compounds such as sacrificial agents (e.g., NaOH, Na_2CO_3, etc.), nonaqueous solvents (e.g., acetonitrile, dimethyl sulfoxide, dimethylformamide, etc.) or ionic liquids. Light distribution can be achieved by external or internal

illumination. Externally illuminated slurry photoreactors can be illuminated from the sides or from the top. This type of photoreactor is usually used to obtain the basic kinetic data and to allow the design of large reactors.

Slurry photoreactors (or fluidized-bed photoreactors) show several advantages, such as uniform illumination throughout the reactor, high mass transfer among photocatalysts and reactants, low amount of catalysts used, inexpensive large-scale construction, etc. However, their main disadvantage is the low distribution of light on the catalyst particles, the difficult separation of the catalyst particles from the reaction mixture (low degree of recycling), and the difficult separation of the products. The strong light absorption of organic species and catalyst particles can limit the penetration depth of UV light into the reaction medium [89]. Since most of the light irradiation is lost due to absorption by the liquid, a large proportion of the catalyst surface area might be inactive due to the low photon energy received [90]. Another problem is the low solubility of gaseous CO_2 in liquid water as a reducing agent. The photocatalyst is mostly suspended in a solid state by a magnetic stirrer. The photocatalyst concentration and particle size play an important role in achieving maximum efficiency for the photocatalytic conversion of CO_2.

3.2. Fixed Bed Photoreactors

In fixed-bed reactors, the catalyst is immobilized on fixed supports, such as beads, plates, fibres, or monoliths. These photoreactors are usually used in the gas–solid reaction systems, where the reducing agents (H_2O and/or H_2) enter the gas phase together with CO_2. The main gas-phase products produced in such photoreactors are mainly CH_4 and CO. The advantage of these photoreactors is that the photocatalyst separation can be avoided since the photocatalyst is deposited on the support matrix inside the reactor around the light source or directly on the walls of the photoreactor. However, in this type of photoreactor, light distribution becomes a limiting factor, depending on the geometry of the light source and the distance between the light source and the photocatalyst. Figure 4 shows various designs of fixed-bed photoreactors, with most attention given to the monolithic photoreactor, the optical fibre photoreactor, and the internally illuminated monolithic photoreactor.

Optical fibres in optical fibre photoreactors have a double function, they transmit light and serve as a support for the photocatalyst, respectively [89]. The advantage of using optical fibres would be a uniform distribution of light on the surface of the photocatalyst and an increase in photon-conversion efficiency. However, the disadvantage of optical fibres is that they are thin and, therefore, can only provide a small surface area of the coating support [91].

A monolith reactor contains monolith structures which are characterized by channel shape, cell density, and wall thickness. In catalytic-reaction engineering, a monolith is defined as a single block of catalyst-containing material through which channels of reactants and products are transported by convection. Monoliths can be used as such (the wall material is the catalyst or catalyst support) or the catalytic material is placed as a layer at the monolith walls (usually by washcoating) [92]. A large specific surface relative to the total volume, low resistance to mass transfer by interphase diffusion, insignificant resistance to the mass transfer within the catalytic layer, high thermal stability, and the fact that the catalyst does not need to be separated from the reaction products are basic features of monoliths. A monolith reactor can take advantage of the unique honeycomb shape of a ceramic monolith, which provides a high surface-to-volume ratio and allows high flow rates with low-pressure drop. However, the efficiency of the monolith is hindered since limited light can penetrate through the cells of the honeycomb substrate. In order to overcome the obstacle of limited light penetration, a honeycomb structure of the monolith was inserted with optical fibres [93]. Liou et al. used a $NiO/InTaO_4$ layer on the top of a precoated SiO_2 sublayer on the internal channels of the monolith. After being carved on the monolith surface, the polymethylmethacrylate (PMMA) optical fibres could transmit and scatter light to effectively illuminate the catalyst inside its channels. The yield of methanol during the

photocatalytic reduction of CO_2 with H_2O was 0.16 mmol g^{-1} h^{-1}. More importantly, the quantum efficiency in the monolith reactor was significantly improved compared to the previous optical-fibre photoreactor.

3.3. Membrane Photoreactors

Membrane reactors usually integrate a membrane, a photocatalyst, and, sometimes, an electrocatalyst. In addition, depending on the type of photocatalytic bed, they can be divided into fixed-bed and slurry photoreactors. Generally, they are used to perform controlled reactions separately and do not allow the mixing of products or reactants and solutions. The transfer of electrons, protons, or holes occurs between the chambers. In addition to the previously described types of photoreactors, membrane reactors also have corresponding advantages and disadvantages, but one of the main problems limiting their efficiency is membrane fouling [19].

3.4. Solar Photoreactors

As is well known, the most unique form of renewable energy is solar energy, which is also the most available energy source on Earth. Therefore, the use of this energy source in the development of solar reactors contributes to further minimizing the energy demand and the environmental crisis. For this reason, special attention has been paid recently to the development of sustainable technologies to produce fuels as well as value-added chemicals, based on the combined use of solar energy as a driving force and CO_2 resources [94,95]. Such technologies are not only sustainable, environmentally friendly, and economically acceptable but also carbon neutral [96]. The classification of solar CO_2 conversion methods and a comparative analysis of various solar photoreactors for the reduction of CO_2 to CH_3OH, including the effect of different influencing parameters (e.g., reactor configuration, operating conditions, and solar-light concentrator) on the performance of the solar photoreactor was recently given in an excellent review [95]. The main problems on which the overall efficiency of solar-driven CO_2 reduction depends are mainly related to the relatively low solar-to-fuel chemical (STC) energy-conversion efficiency (usually < 2%), poor product selectivity, and in some cases, to the inefficient use of the total volume of the solar photoreactor [94,95]. Generally, the solar-energy conversion efficiency is strongly dependent on the cumulative effect of different consecutive steps, including the light-absorption efficiency, the charge excitation/separation efficiency, the charge migration and transport efficiency, and the charge utilization efficiency for photocatalytic reactions [97]. Therefore, all of these processes' steps must be considered and optimized to design a highly efficient photocatalyst. Furthermore, the overall efficiency of the photoreduction of CO_2 to fuels can be improved through an engineering approach towards reactor configuration and design aspects [19]. For example, the problem related to the transformation of solar light radiation into useful energy can be solved by using different devices, such as mirrors, flat-sheet reflectors, compound parabola, Frensel lens concentrator, etc. for capturing solar light and to provide high-flux solar radiation [95]. Concentrated solar photoreactors enable effective solar-light utilization and higher efficiency than other types of solar photoreactors due to the possibility of reaching the maximum intensity of sunlight [95]. According to the expectations, the development of hybrid solar photoreactors, which combine the advantages of the slurry, membrane, and concentrated solar photoreactors, would probably result in improved solar CO_2 photoreduction with a desired product yield [95].

3.5. Modelling and Scale up of the Photoreactor

Modelling and reactor design should allow an easy transition from lab-scale systems to industrial setups. There are two basic approaches to the reactor design. The first is the traditional one, based on empirical methodology which means long-term experimental research, starting with laboratory reactors and ending with reactors of finite dimensions, depending on the field of application. Another approach is a numerical one, based on the application of mathematical models and simulations, which, thanks to the increasing

availability of commercial and open-source software, shortens the time required for the development of photocatalytic technologies and reduces investments for research purposes.

Modelling is an irreplaceable tool for understanding the effects of the transition from laboratory scale to full-scale plants and different operating conditions. For modelling photocatalytic reactions, the multiscale modelling approach is often used, where conceptual and computational modelling scales are considered. Conceptual modelling means studying a specific subset of the process by a specialised model, while computational modelling overcomes hardware throughput. Each modelling scale involves four distinct steps: radiation model, kinetic model, mass balances, and experimental results. The only difference is in the experimental results, which at the lab scale are used to estimate the kinetic parameters, while overall design and validation are considered at the large scale.

To determine the behaviour on the photocatalytic material surface for the smallest-scale models (quantum level) the density functional theory (DFT) is often used. To estimate reaction kinetics, kinetic Monte-Carlo (kMC) and mean-field microkinetic modelling (MKM) can be used, after a rough estimation of reaction-rate constants, preferably supported by experimental data for comparison and validation. Computational fluid dynamics (CFD) can be used to simulate large-scale reactors in terms of reactor design and optimised operating conditions [98].

A multiphysics model was developed by using COMSOL, where the computational fluid-dynamic model was combined with the novel CO_2 photoreduction intrinsic-reaction kinetic model based on gas adsorption, surface reactions, and desorption, while the Gaussian distribution model and the Beer–Lambert model were used to simulate of UV-light intensity distribution. They found similar simulation and experimental results for methane, carbon monoxide, and hydrogen yield in the concentration range of 10^{-4} mol m^{-3} at low CO_2 and H_2O moisture partial pressure. The simulation shows that with increasing CO_2 partial pressure, the CH_4 and H_2 yields decrease, and the CO yield increases, while with increasing H_2O partial pressure, the CH_4 and H_2 yields increase and CO decreases. The adsorption sites and equilibrium constant, temperature, and UV lighting affect the surface concentration, and thus the CH_4, CO, and H_2 yields. Gas adsorption on the photocatalyst surface is one of the crucial steps to improve the CH_4 yield in the CO_2 photoreduction process [99].

Recently, Xiong et al. [100] developed a novel twin reactor for the simultaneous reactions of CO_2 hydrogenation and water splitting in the gas and liquid phases, respectively. They found that the H_2 produced during water splitting effectively enhanced the CO_2 hydrogenation into the gas phase and that the highest CO_2 reduction activity was achieved by using Pt/TiO_2 and Cu/TiO_2, which promoted H_2 evolution and CO_2 hydrogenation and led to enhanced CO_2 photoreduction.

Khan and Tahir have reviewed the slurry, fixed bed, and membrane photoreactors based on their operational mode, type of bed, number of phases involved, the membrane used, and type of light source. The influence of factors such as light position and distribution, the material of construction, temperature, and pressure on fuel production has also been explained [19].

4. Challenges and Recommendations

There are a few challenges in the photocatalytic conversion of CO_2 which include charge separation and the creation of electron-hole pairs, visible-light activation of the semiconductor, increasing selectivity to desired products, and improving the efficiency of photocatalysts in terms of products yields. It is a great effort for scientists to look at and compare all the previous research and provide guidelines to improve the previous results of photocatalytic conversion of CO_2, as there are many variables that affect the process itself. For example, different types of photoreactors, different methods and reaction conditions of photocatalyst synthesis, light sources, and many others are used. The increasing demand for green energy is also a major challenge from the photochemical point of view. In this context, many suitable photocatalysts have been prepared, but the photocatalytic conversion of

CO_2 is energy consuming and a very complex process because there are several possible reaction pathways leading to different products.

The next major challenge is to produce high-value fuels and chemicals by the photocatalytic conversion of CO_2 on an industrial scale. Solar-driven CO_2 reduction (CO_2 RR) with H_2O or H_2 is proving to be a promising approach for the production of various monocarbon C_1 and multicarbon C_{2+} products, as it relies on naturally available solar energy to drive the reaction. As previously pointed out, many achievements have been achieved through the rational design of photocatalysts, the application of different designs of photoreactors and the use of process-engineering methodology. However, the potential for CO_2 photoreduction on an industrial scale is largely limited by the regional solar intensity that depends on geographic location. Recent technological advances in the field of photo-assisted CO_2 reduction include various strategies and approaches, the most studied of which are photocatalysis (PC), photoelectrocatalysis (PEC), and photovoltaic-integrated systems [94–101]. In the photocatalytic process, simultaneous activation, and reduction of CO_2 by photogenerated electrons in the conductive band and oxidation of H_2O on photogenerated holes in the valence band should be carried out. However, this limits the use of wide-bandgap semiconductors to meet the redox potential requirement for CO_2 reduction and H_2O oxidation. Moreover, they cannot effectively absorb light in the visible light region, which significantly limits solar-to-fuel efficiency. Compared to the photocatalytic process, the photoelectrode-based PEC reduction of CO_2 can promote charge-carrier separation and allow the use of narrow-bandgap photocathodes to extend light absorption, leading to the increase of the solar-to-fuel efficiency to 1–5% [94,101]. In the past few years, the attention of researchers has been focused on integrated systems such as photovoltaic-biased photoelectrocatalysis (PV-PEC) and photovoltaic-powered electrocatalysis (PV-EC) for CO_2RR, which directly couples a photovoltainc (PV) cell with an electrochemical (EC) or photoelectrochemical (PEC) cell [94,101–104]. Comparing PV-PEC and PV-EC CO_2 RR for the same PV cell and for the same group of products, Zhang et al. [104] demonstrate that PV-PEC CO2RR have higher solar-to-chemical (STC) energy-conversion efficiency (8%) than PV-EC.

5. Conclusions

Photocatalytic processes represent one of the most environmentally friendly ways to solve the problem of global warming caused by the emission of enormously high concentrations of CO_2. The advantage of photocatalytic conversion of CO_2 to renewable fuels over other methods is the use of most agents that are available in nature in large quantities, the reactions take place at room temperature, which is energetically more favourable compared to thermal processes. In this review, numerous possibilities for the synthesis of new photocatalysts based on metal oxides, the Z-scheme heterojunction composites, MOFs, carbon nitrides, and layered double hydroxide are presented, as well as their efficiency and selectivity in photocatalytic CO_2 reduction. Among all semiconductors, TiO_2 and its composites prepared in different ways (described in detail in the paper) have been studied the most. The synthesis of new photocatalytic composites and the proper design of photoreactors, as well as the prediction of the reaction mechanism of the reaction, can improve photocatalytic performance regarding the mass transfer and absorption of light by the photocatalyst. Future research and commercialization of solar-driven CO_2 reduction are expected to be focused on the development of integrated systems such as PV-PEC and PV-EC CO_2 RR that will ensure high solar-to-full efficiency and ensure low operational costs.

Author Contributions: Both authors contributed equally to this work. All authors have read and agreed to the published version of the manuscript.

References

1. Li, D.; Kassymova, M.; Cai, X.; Zang, S.-Q.; Jiang, H.-L. Photocatalytic CO_2 reduction over metal-organic framework-based materials. *Coord. Chem. Rev.* **2020**, *412*, 213262. [CrossRef]
2. IEA. Global Energy Review: CO_2 Emissions in 2021. International Energy Agency. March 2022. Available online: https://www.iea.org/reports/global-energy-review-co2-emissions-in-2021-2 (accessed on 28 October 2022).
3. Tiseo, I. Breakdown of CO2 Emissions in the EU-27 2020, by Sector. 2023. Available online: https://www.statista.com/statistics/1240108/road-transportation-greenhouse-gas-emissions-eu/?locale=en (accessed on 16 February 2023).
4. US EPA. Sources of Greenhouse Gas Emissions. Available online: https://www.epa.gov/ghgemissions/sources-greenhouse-gas-emissions (accessed on 28 October 2022).
5. Albo, J.; Luis, P.; Irabien, A. Carbon dioxide capture from flue gases using a crossflow membrane contactor and the ionic liquid 1-ethyl-3-methylimidazolium ethylsulfate. *Ind. Eng. Chem. Res.* **2010**, *49*, 11045–11051. [CrossRef]
6. He, M.; Sun, Y.; Han, B. Green carbon science: Scientific basis for integrating carbon resource processing, utilization, and recycling. *Angew. Chem. Int. Ed.* **2013**, *52*, 9620–9633. [CrossRef]
7. Putting CO2 to Use: Creating Value from Emissions. International Energy Agency (IEA): Paris, France, 2019; p. 86. Available online: https://iea.blob.core.windows.net/assets/50652405-26db-4c41-82dc-c23657893059/Putting_CO2_to_Use.pdf (accessed on 16 February 2023).
8. Zhong, J.; Yang, X.; Wu, Z.; Liang, B.; Huang, Y.; Zhang, T. State of the art and perspectives in heterogeneous catalysis of CO_2 hydrogenation to methanol. *Chem. Soc. Rev.* **2020**, *49*, 1385–1413. [CrossRef]
9. Choi, W.; Dong, F.; Hatzell, M. Solar Energy Utilization and Photo(electro)catalysis for Sustainable Environment. *ACS EST Engg.* **2022**, *2*, 940–941. [CrossRef]
10. Hong, J.; Zhang, W.; Ren, J.; Xu, R. Photocatalytic reduction of CO_2: A brief review on product analysis and systematic methods. *Anal. Methods* **2013**, *5*, 1086–1097. [CrossRef]
11. Lu, H.; Wang, Z.; Wang, L. Photocatalytic and Photoelectrochemical Carbon Dioxide Reductions toward Value-Added Multicarbon Products. *ACS EST Eng.* **2022**, *2*, 975–988. [CrossRef]
12. Levinson, R.; Berdahl, P.; Akbari, H. Solar Spectral Optical Properties of Pigments—Part I: Model for Deriving Scattering and Absorption Coefficients from Transmittance and Reflectance Measurements. *Sol. Energy Mater. Sol. Cells* **2005**, *89*, 319–349. [CrossRef]
13. Kovacic, Z.; Likozar, B.; Hus, M. Photocatalytic CO_2 reduction: A review of ab initio mechanism, kinetics, and multiscale modeling simulations. *ACS Catal.* **2020**, *10*, 14984–15007. [CrossRef]
14. Hemminger, J.C.; Carr, R.; Somorjai, G.A. The photoassisted reaction of gaseous water and carbon dioxide adsorbed on the $SrTiO_3$ (111) crystal face to form methane. *Chem. Phys. Lett.* **1978**, *57*, 100–104. [CrossRef]
15. Wang, M.; Zeng, S.; Woldu, A.R.; Hu, L. $BiVO_4/Bi_2S_3$ Z-scheme heterojunction with MnO_x as a cocatalyst for efficient photocatalytic CO_2 conversion to methanol by pure water. *Nano Energy* **2022**, *104*, 107925. [CrossRef]
16. Yang, Y.; Pan, Y.-X.; Tu, X.; Liu, C.-J. Nitrogen doping of indium oxide for enhanced photocatalytic reduction of CO_2 to methanol. *Nano Energy* **2022**, *101*, 107613. [CrossRef]
17. Shekar, G.C.S.; Alkanad, K.; Thejaswini, B.; Alnaggar, G.; Al Zaqri, N.; Drmosh, Q.; Boshaala, A.; Lokanath, N.K. Alkaline mediated sono-synthesis of surface oxygen-vacancies-rich cerium oxide for efficient photocatalytic CO_2 reduction to methanol. *Surf. Interfaces* **2022**, *34*, 102389.
18. Tahir, M.; Amin, N.S. Advances in visible light responsive titanium oxide-based photocatalysts for CO_2 conversion to hydrocarbon fuels. *Energy Convers. Manag.* **2013**, *76*, 194–214. [CrossRef]
19. Khan, A.A.; Tahir, M. Recent advancements in engineering approach towards design of photoreactors for selective photocatalytic CO_2 reduction to renewable fuels. *J. CO2 Util.* **2019**, *29*, 205–239. [CrossRef]
20. Heng, H.; Gan, Q.; Meng, P.; Liu, X. $H_3PW_{12}O_{40}/TiO_2$-In_2O_3: A visible light driven type-II heterojunction photocatalyst for the photocatalytic degradation of imidacloprid. *RSC Adv.* **2016**, *6*, 73301. [CrossRef]
21. Channei, D.; Chansaenpak, K.; Phanichphant, S.; Jannoey, P.; Khanitchaidecha, W.; Nakaruk, A. Synthesis and Characterization of WO_3/CeO_2 Heterostructured Nanoparticles for Photodegradation of Indigo Carmine Dye. *ACS Omega* **2021**, *6*, 19771–19777. [CrossRef]
22. Yang, L.; Liu, Z. Study on light intensity in the process of photocatalytic degradation of indoor gaseous formaldehyde for saving energy. *Energy Convers. Manag.* **2007**, *48*, 882–889. [CrossRef]
23. Pan, B.; Wu, Y.; Rhimi, B.; Qin, J.; Huang, Y.; Yuan, M.; Wang, C. Oxygen-Doping of $ZnIn_2S_4$ Nanosheets Towards Boosted Photocatalytic CO_2 Reduction. *J. Energy Chem.* **2021**, *57*, 1–9. [CrossRef]
24. Jiang, Y.; Yu, Y.; Zhang, X.; Weinert, M.; Song, X.; Ai, J.; Han, L.; Fei, H. N-Heterocyclic Carbene-Stabilized Ultrasmall Gold Nanoclusters in a Metal-Organic Framework for Photocatalytic CO_2 Reduction. *Angew. Chem. Int. Ed.* **2021**, *60*, 17388–17393. [CrossRef]
25. Li, D.; Hussain, S.; Wang, Y.; Huang, C.; Li, P.; Wang, M.; He, T. ZnSe/CdSe Z-Scheme Composites with Se Vacancy for Efficient Photocatalytic CO_2 Reduction. *Appl. Catal. B* **2021**, *286*, 119887. [CrossRef]
26. Tran, D.P.H.; Pham, M.-T.; Bui, X.-T.; Wang, Y.-F.; You, S.-J. CeO₂ as a photocatalytic material for CO_2 conversion: A review. *Sol. Energy* **2022**, *240*, 443–466. [CrossRef]

27. Xia, X.H.; Jia, Z.H.; Yu, Y.; Liang, Y.; Wang, Z.; Ma, L.L. Preparation of multi-walled carbon nanotube supported TiO_2 and its photocatalytic activity in the reduction of CO_2 with H_2O. *Carbon* **2007**, *45*, 717–721. [CrossRef]

28. Ai, Z.H.; Ho, W.K.; Lee, S. Efficient visible light photocatalytic removal of NO with BiOBr–graphene nanocomposites. *J. Phys. Chem. C* **2011**, *115*, 25330–25337. [CrossRef]

29. Woolerton, T.W.; Sheard, S.; Pierce, E.; Ragsdale, S.W.; Armstrong, F.A. CO_2 photoreduction at enzyme-modified metal oxide nanoparticles. *Energy Environ. L Sci.* **2011**, *4*, 2393–2399. [CrossRef]

30. Ettedgui, J.; Diskin-Posner, Y.; Weiner, L.; Neumann, R. Photoreduction of carbon dioxide to carbon monoxide with hydrogen catalyzed by a rhenium(I) phenanthroline–polyoxometalate hybrid complex. *J. Am. Chem. Soc.* **2010**, *133*, 188–190. [CrossRef]

31. Rehman, Z.U.; Bilal, M.; Hou, J.; Butt, F.K.; Ahmad, J.; Ali, S.; Hussain, A. Photocatalytic CO_2 Reduction Using TiO_2-Based Photocatalysts and TiO_2 Z-Scheme Heterojunction Composites: A Review. *Molecules* **2022**, *27*, 2069. [CrossRef]

32. Chang, X.; Wang, T.; Gong, J. CO_2 photo-reduction: Insights into CO_2 activation and reaction on surfaces of photocatalysts. *Energy Environ. Sci.* **2016**, *9*, 2177–2196. [CrossRef]

33. Li, X.; Yu, J.; Jaroniec, M.; Chen, X. Cocatalysts for Selective Photoreduction of CO_2 INTO Solar Fuels. *Chem. Rev.* **2019**, *119*, 3962–4179. [CrossRef]

34. Kong, T.; Jiang, Y.; Xiong, Y. Photocatalytic CO_2 conversion: What can we learn from conventional CO_x hydrogenation? *Chem. Soc. Rev.* **2020**, *49*, 6579–6591. [CrossRef] [PubMed]

35. Xu, X.; Asakura, H.; Hosokawa, S.; Tanaka, T.; Teramura, K. Tuning Ag-modified $NaTaO_3$ to achieve high CO selectivity for the photocatalytic conversion of CO_2 using H_2O as the electron donor. *Appl. Catal. B Environ.* **2023**, *320*, 121885. [CrossRef]

36. Peng, C.; Reid, G.; Wang, H.; Hu, P. Perspective: Photocatalytic reduction of CO_2 to solar fuels over semiconductors. *J. Chem. Phys.* **2017**, *147*, 030901. [CrossRef]

37. Almomani, F.; Bhosale, R.; Khraisheh, M.; Kumar, A.; Tawalbeh, M. Photocatalytic conversion of CO_2 and H_2O to useful fuels by nanostructured composite catalysis. *Appl. Surf. Sci.* **2019**, *483*, 363–372. [CrossRef]

38. Inoue, T.; Fujishima, A.; Konishi, S.; Honda, K. Photoelectrocatalytic reduction of carbon dioxide in aqueous suspensions of semiconductor powders. *Nature* **1979**, *277*, 637–638. [CrossRef]

39. Wang, Y.; Chen, E.; Tang, J. Insight on Reaction Pathways of Photocatalytic CO_2 Conversion. *ACS Catal.* **2022**, *12*, 7300–7316. [CrossRef]

40. Olivo, A.; Ghedini, E.; Signoretto, M.; Compagnoni, M.; Rossetti, I. Liquid vs. Gas Phase CO_2 Photoreduction Process: Which Is the Effect of the Reaction Medium? *Energies* **2017**, *10*, 1394. [CrossRef]

41. Gao, Y.; Liu, S.; Zhao, Z.; Tao, H.; Sun, Z. Heterogeneous catalysis of CO_2 hydrogenation to C_{2+} products. *Acta Phys.-Chim. Sin.* **2018**, *34*, 858–872. [CrossRef]

42. Li, W.; Wang, H.; Jiang, X.; Zhu, J.; Liu, Z.; Guo, X.; Song, C. A short review of recent advances in CO_2 hydrogenation to hydrocarbons over heterogeneous catalysts. *RCS Adv.* **2018**, *8*, 7651–7669. [CrossRef]

43. Chen, Y.-X.; Xu, Y.-F.; Wang, X.-D.; Chen, H.-Y.; Kuang, D.-B. Solvent selection and Pt decoration towards enhanced photocatalytic CO_2 reduction over $CsPbBr_3$ perovskite single crystals. *Sustain. Energy Fuels* **2020**, *4*, 2249–2255. [CrossRef]

44. Ola, O.; Maroto-Valer, M.M. Review of material design and reactor engineering on TiO_2 photocatalysis for CO_2 reduction. *J. Photochem. Photobiol. C Photochem. Rev.* **2015**, *24*, 16–42. [CrossRef]

45. Wang, Y.; Huang, N.Y.; Shen, J.Q.; Liao, P.Q.; Chen, X.M.; Zhang, J.P. Hydroxide ligands cooperate with catalytic centers in metal–organic frameworks for efficient photocatalytic CO_2 reduction. *J. Am. Chem. Soc.* **2018**, *140*, 38–41. [CrossRef] [PubMed]

46. Zhang, K.; Gao, Q.; Xu, C.; Zhao, D.; Zhu, Q.; Zhu, Z.; Wang, J.; Liu, C.; Yu, H.; Sun, C.; et al. Current dilemma in photocatalytic CO_2 reduction: Real solar fuel production or false positive outcomings? *Carbon Neutrality* **2022**, *1*, 10. [CrossRef]

47. Das, R.; Chakraborty, S.; Peter, S.C. Systematic assessment of solvent selection in photocatalytic CO_2 reduction. *ACS Energy Lett.* **2021**, *6*, 3270–3274. [CrossRef]

48. Liu, B.J.; Torimoto, T.; Yoneyama, H. Photocatalytic reduction of CO_2 using surface-modified CdS photocatalysts in organic solvents. *J. Photochem. Photobiol. A Chem.* **1998**, *113*, 93–97. [CrossRef]

49. Alcasabas, A.; Ellis, P.R.; Malone, I.; Williams, G.; Zalitis, C. A Comparison of Different Approaches to the Conversion of Carbon Dioxide into Useful Products: Part I: CO_2 reduction by electrocatalytic, thermocatalytic and biological routes. *Johns. Matthey Technol. Rev.* **2021**, *65*, 180–196. [CrossRef]

50. Rajalakshmi, K.; Jeyalakshmi, V.; Krishnamurthy, K.R.; Viswanathan, B. Photocatalytic reduction of carbon dioxide by water on titania: Role of photophysical and structural properties. *Indian J. Chem.* **2012**, *51A*, 411–419.

51. Wei, Y.; Jiao, J.; Zhao, Z.; Zhong, W.; Li, J.; Liu, J.; Jiang, G.; Duan, A. 3D ordered macroporous TiO_2-supported Pt@ CdS core–shell nanoparticles: Design, synthesis and efficient photocatalytic conversion of CO_2 with water to methane. *J. Mater. Chem. A* **2015**, *3*, 11074–11085. [CrossRef]

52. Cheng, X.; Wang, P.; Liu, H. Visible-light-driven photoelectrocatalytic degradation of diclofenac by N, S-TiO_2/TiO_2NTs photoelectrode: Performance and mechanism study. *J. Environ. Chem. Eng.* **2015**, *3*, 1713–1719. [CrossRef]

53. Yahaya, A.H.; Gondal, M.A.; Hameed, A. Selective laser enhanced photocatalytic conversion of CO_2 into methanol. *Chem. Phys. Lett.* **2004**, *400*, 206–212. [CrossRef]

54. Zhou, Y.; Tian, Z.; Zhao, Z.; Liu, Q.; Kou, J.; Chen, X.; Gao, J.; Yan, S.; Zou, Z. High-yield synthesis of ultrathin and uniform $Bi2WO_6$ square nanoplates benefitting from photocatalytic reduction of CO_2 into renewable hydrocarbon fuel under visible light. *ACS Appl. Mater. Interfaces* **2011**, *3*, 3594–3601. [CrossRef]

55. Zhao, C.; Krall, A.; Zhao, H.; Zhang, Q.; Li, Y. Ultrasonic spray pyrolysis synthesis of Ag/TiO$_2$ nanocomposite photocatalysts for simultaneous H$_2$ production and CO$_2$ reduction. *Int. J. Hydrogen Energy* **2012**, *37*, 9967–9976. [CrossRef]

56. Yang, X.Y.; Xiao, T.C.; Edwards, P.P. The use of products from CO$_2$ photoreduction for improvement of hydrogen evolution in water splitting. *Int. J. Hydrogen Energy* **2011**, *36*, 6546–6552. [CrossRef]

57. Razzaq, A.; In, S.-I. TiO$_2$ Based Nanostructures for Photocatalytic CO$_2$ Conversion to Valuable Chemicals. *Micromachines* **2019**, *10*, 326. [CrossRef]

58. Albero, J.; Peng, Y.; García, H. Photocatalytic CO$_2$ Reduction to C$_{2+}$ Products. *ACS Catal.* **2020**, *10*, 5734–5749. [CrossRef]

59. Camarillo, R.; Rizaldos, D.; Jiménez, C.; Martínez, F.; Rincón, J. Enhancing the photocatalytic reduction of CO$_2$ with undoped and Cu-doped TiO$_2$ nanofibers synthesized in supercritical medium. *J. Supercrit. Fluids* **2019**, *147*, 70–80. [CrossRef]

60. Shen, M.; Zhang, L.; Wang, M.; Tian, J.; Jin, X.; Guo, L.; Wang, L.; Shi, J. Carbon-vacancy modified graphitic carbon nitride: Enhanced CO$_2$ photocatalytic reduction performance and mechanism probing. *J. Mater. Chem. A* **2019**, *7*, 1556. [CrossRef]

61. Wang, Q.; Zhang, L.; Guo, Y.; Shen, M.; Wang, M.; Li, B.; Shi, J. Multifunctional 2D porous g-C$_3$N$_4$ nanosheets hybridized with 3D hierarchical TiO$_2$ microflowers for selectuive dye adsorption, antibiotic degradation and CO$_2$ reduction. *Chem. Eng. J.* **2020**, *396*, 125347. [CrossRef]

62. Guo, Y.; Wang, Q.; Wang, M.; Shen, M.; Zhang, L. FeP modified polymeric carbon nitride as a noble-metal free photocatalyst for efficient CO$_2$ reduction. *Catal. Comm.* **2021**, *156*, 106326. [CrossRef]

63. Feng, S.; Zhao, J.; Bai, Y.; Liang, X.; Wang, T.; Wang, C. Facile synthesis of Mo-doped TiO$_2$ for selective photocatalytic CO$_2$ reduction to methane: Promoted H$_2$O dissociation by Mo doping. *J. CO2 Util.* **2020**, *38*, 1–9. [CrossRef]

64. Molina-Muriel, M.; Peng, Y.; García, H.; Ribera, A. Increased photocatalytic activity and selectivity towards methane of trimetallic NiTiAl-LDH. *J. Alloys Compd.* **2022**, *897*, 163124. [CrossRef]

65. Wang, X.; Ng, D.; Du, H.; Hornung, C.H.; Polyzos, A.; Seeber, A.; Li, H.; Huo, Y.; Xie, Z. Copper decorated indium oxide rods for photocatalytic CO$_2$ conversion under simulated sun light. *J. CO2 Util.* **2022**, *58*, 101909. [CrossRef]

66. Tahir, B.; Tahir, M.; Nawawi, M.G.M. Highly stable honeycomb structured 2D/2D vanadium aluminum carbide MAX coupled g-C$_3$N$_4$ composite for stimulating photocatalytic CO$_2$ reduction to CO and CH$_4$ in a monolith photoreactor. *J. Alloys Compd.* **2022**, *927*, 166908. [CrossRef]

67. Movahed, S.K.; Najinasab, A.; Nikbakht, R.; Dabiri, M. Visible light assisted photocatalytic reduction of CO$_2$ to methanol using Fe$_3$O$_4$@NC/Cu$_2$O nanostructure photocatalyst. *J. Photochem. Photobiol. A Chem.* **2020**, *401*, 112763. [CrossRef]

68. Cheng, M.; Bai, S.; Xia, Y.; Zhu, X.; Chen, R.; Liao, Q. Highly efficient photocatalytic conversion of gas phase CO$_2$ by TiO$_2$ nanotube array sensitized with CdS/ZnS quantum dots under visible light. *Int. J. Hydrogen Energy* **2021**, *46*, 31634–31646. [CrossRef]

69. Li, M.; Liu, Z.; Wu, S.; Zhang, J. Advances for CO$_2$ Photocatalytic Reduction in Porous Ti-Based Photocatalysts. *ACS EST Eng.* **2022**, *2*, 942–956. [CrossRef]

70. Liu, G.; Hoivik, N.; Wang, K.; Jakobsen, H. Engineering TiO$_2$ nanomaterials for CO$_2$ conversion/solar fuels. *Sol. Energy Mater. Sol. Cell.* **2012**, *105*, 53–68. [CrossRef]

71. Sanz-Marco, A.; Hueso, J.L.; Sebastian, V.; Nielsen, D.; Mossin, S.; Holgado, J.P.; Bueno-Alejo, C.J.; Balas, F.; Santamaria, J. LED-driven controlled deposition of Ni onto TiO$_2$ for visible-light expanded conversion of carbon dioxide into C$_1$–C$_2$ alkanes. *Nanoscale Adv.* **2021**, *3*, 3788. [CrossRef]

72. Zeng, L.; Chen, J.-W.; Zhong, L.; Zhen, W.; Tay, Y.Y.; Li, S.; Wang, Y.-G.; Huang, L.; Xue, C. Synergistic effect of Ru-N4 sites and Cu-N3 sites in carbon nitride for highly selective photocatalytic reduction of CO$_2$ to methane. *Appl. Catal. B Environ.* **2022**, *307*, 121154. [CrossRef]

73. Wang, C.; Zhao, Y.; Xu, H.; Li, Y.; Wei, Y.; Liu, J.; Zhao, Z. Efficient Z-scheme photocatalysts of ultrathin g-C$_3$N$_4$-wrapped Au/TiO$_2$-nanocrystals for enhanced visible-light-driven conversion of CO$_2$ with H$_2$O. *Appl. Catal. B Environ.* **2020**, *263*, 118314. [CrossRef]

74. Sonowal, K.; Saikia, L. Metal–organic frameworks and their composites for fuel and chemical production via CO$_2$ conversion and water splitting. *RSC Adv.* **2022**, *12*, 11686–11707. [CrossRef]

75. Qian, Y.; Zhang, F.; Pang, H. A Review of MOFs and Their Composites-Based Photocatalysts: Synthesis and Applications. *Adv. Funct. Mater.* **2021**, *31*, 2104231. [CrossRef]

76. Dhakshinamoorthy, A.; Li, Z.; Garcia, H. Catalysis and photocatalysis by metal organic frameworks. *Chem. Soc. Rev.* **2018**, *47*, 8134–8172. [CrossRef] [PubMed]

77. Sonowal, K.; Nandal, N.; Basyach, P.; Kalita, L.; Jain, S.L.; Saikia, L. Photocatalytic reduction of CO$_2$ to methanol using Zr(IV)-based MOF composite with g-C$_3$N$_4$ quantum dots under visible light irradiation. *J. CO2 Util.* **2022**, *57*, 101905. [CrossRef]

78. Zhan, W.; Gao, H.; Yang, Y.; Li, X.; Zhu, Q.-L. Rational Design of Metal–Organic Framework-Based Materials for Photocatalytic CO$_2$ Reduction. *Adv. Energy Sustain. Res.* **2022**, *3*, 2200004. [CrossRef]

79. Fu, Y.; Sun, D.; Chen, Y.; Huang, R.; Ding, Z.; Fu, X.; Li, Z. An Amine-Functionalized Titanium Metal–Organic Framework Photocatalyst with Visible-Light-Induced Activity for CO$_2$ Reduction. *Angew. Chem. Int. Ed.* **2012**, *51*, 3364–3367. [CrossRef]

80. Laurier, K.G.M.; Vermoortele, F.; Ameloot, R.; De Vos, D.E.; Hofkens, J.; Roeffaers, M.B.J. Iron(III)-based metal-organic frameworks as visible light photocatalysts. *J. Am. Chem. Soc.* **2013**, *135*, 14488–14491. [CrossRef] [PubMed]

81. Wang, G.; Sun, Q.; Liu, Y.; Huang, B.; Dai, Y.; Zhang, X.; Qin, X. A bismuth-based metal-organic framework as an efficient visible-light-driven photocatalyst. *Chemistry* **2015**, *21*, 2364–2367. [CrossRef]

82. Xiao, J.D.; Jiang, H.L. Metal-organic frameworks for photocatalysis and photothermal catalysis. *Acc. Chem. Res.* **2019**, *52*, 356–366. [CrossRef] [PubMed]

83. Huang, P.; Huang, J.; Li, J.; Pahm, T.D.; Zhang, L.; He, J.; Brudvig, G.W.; Deskins, N.A.; Frenkel, A.I.; Li, G. Revealing the structure of single cobalt sites in carbon nitride for photocatalytic CO_2 reduction. *J. Phys. Chem. C* **2022**, *126*, 8596–8604. [CrossRef]

84. Xia, P.; Antonietti, M.; Zhu, B.C.; Heil, T.; Yu, J.G.; Cao, S.W. Designing Defective Crystalline Carbon Nitride to Enable Selective CO_2 Photoreduction in the Gas Phase. *Adv. Funct. Mater.* **2019**, *29*, 1900093. [CrossRef]

85. Wang, L.; Yu, J. CO_2 capture and in situ photocatalytic reduction. *Chem. Catal.* **2022**, *2*, 425–438. [CrossRef]

86. Ola, O.; Maroto-Valer, M.M. Synthesis, characterization and visible light photocatalytic activity of metal based TiO_2 monoliths for CO_2 reduction. *Chem. Eng. J.* **2016**, *283*, 1244–1253. [CrossRef]

87. Alalm, M.G.; Djellabi, R.; Meroni, D.; Pirola, C.; Bianchi, C.L.; Boffito, D.C. Toward Scaling-Up Photocatalytic Process for Multiphase Environmental Applications. *Catalysts* **2021**, *11*, 562. [CrossRef]

88. Li, Y.; Ma, Y.; Li, K.; Chen, S.; Yue, D. Photocatalytic Reactor as a Bridge to Link the Commercialization of Photocatalyst in Water and Air Purification. *Catalysts* **2022**, *12*, 724. [CrossRef]

89. Nguyen, T.V.; Wu, J.C. Photoreduction of CO_2 in an optical-fiber photoreactor: Effects of metals addition and catalyst carrier. *Appl. Catal. A Gen.* **2008**, *335*, 112–120. [CrossRef]

90. Mukherjee, P.S.; Ray, A.K. Major challenges in the design of a large-scale photocatalytic reactor for water treatment. *Chem. Eng. Technol. Ind. Chem.-Plant Equip.-Process Eng. -Biotechnol.* **1999**, *22*, 253–260. [CrossRef]

91. Wang, W.; Ku, Y. Photocatalytic degradation of gaseous benzene in air streams by using an optical fiber photoreactor. *J. Photochem. Photobiol. A Chemistry.* **2003**, *159*, 47–59. [CrossRef]

92. Moulijn, J.A.; Kapteijn, F. Monolithic reactors in catalysis: Excellent control. *Curr. Opin. Chem. Eng.* **2013**, *2*, 346–353. [CrossRef]

93. Liou, P.Y.; Chen, S.C.; Wu, J.C.; Liu, D.; Mackintosh, S.; Maroto-Valer, M.; Linforth, R. Photocatalytic CO_2 reduction using an internally illuminated monolith photoreactor. *Energy Environ. Sci.* **2011**, *4*, 1487–1494. [CrossRef]

94. He, J.; Janáky, C. Recent advances in solar-driven carbon dioxide conversion: Expectations versus reality. *ACS Energy Lett.* **2020**, *5*, 1996–2014. [CrossRef]

95. Francis, A.; Shanmuga Priya, S.; Harish Kumar, S.; Sudhakar, K.; Tahir, M. A review on recent developments in solar photoreactors for carbon dioxide conversion to fuels. *J. CO2 Util.* **2021**, *47*, 101515. [CrossRef]

96. Yu, S.; Wilson, A.J.; Kumari, G.; Zhang, X.; Jain, P.K. Opportunities and challenges of solar –energy-driven carbon dioxide to fuel conversion with plasmonic catalysts. *ACS Energy Lett.* **2017**, *2*, 2058–2070. [CrossRef]

97. Li, X.; Yu, J.; Jaroniec, M. Hierarchical photocatalysts. *Chem. Soc. Rev.* **2016**, *45*, 2603. [CrossRef]

98. Ješić, D.; Jurković, D.L.; Pohar, A.; Suhadolnik, L.; Likozar, B. Engineering photocatalytic and photoelectrocatalytic CO_2 reduction reactions: Mechanisms, intrinsic kinetics, mass transfer resistances, reactors and multi-scale modelling simulations. *Chem. Eng. J.* **2021**, *407*, 126799. [CrossRef]

99. Lu, X.; Luo, X.; Thompson, W.A.; Tan, J.Z.; Maroto-Valer, M.M. Investigation of carbon dioxide photoreduction process in a laboratory-scale photoreactor by computational fluid dynamic and reaction kinetic modeling. *Front. Chem. Sci. Eng.* **2022**, *16*, 1149–1163. [CrossRef]

100. Xiong, Z.; Kuang, C.-C.; Lin, K.-Y.; Lei, Z.; Chen, X.; Gong, B.; Yang, J.; Zhao, Y.; Zhang, J.; Xia, B.; et al. Enhanced CO_2 photocatalytic reduction through simultaneously accelerated H_2 evolution and CO_2 hydrogenation in a twin photoreactor. *J. CO2 Util.* **2018**, *24*, 500–508. [CrossRef]

101. Lin, H.; Luo, S.; Zhang, H.; Ye, J. Toward solar-driven carbon recycling. *Joule* **2022**, *6*, 294–314. [CrossRef]

102. Gui, M.M.; Cathie Lee, W.P.; Putri, L.K.; Kong, X.Y.; Tan, L.-L.; Chai, S.P. Photo-Driven Reduction of Carbon Dioxide: A Sustainable Approach Towards Achieving Carbon Neutrality Goal. *Front. Chem. Eng.* **2021**, *3*, 744911. [CrossRef]

103. Boutin, E.; Patel, M.; Kecsenovity, E.; Suter, S.; Janáky, C.; Haussener, S. Photo-Electrochemical Conversion of CO_2 Under Concentrated Sunlight Enables Combination of High Reaction Rate and Efficiency. *Adv. Energy Mater.* **2022**, *12*, 2200585. [CrossRef]

104. Zhang, Y.; Ye, C.; Duan, J.; Feng, H.; Liu, D.; Li, Q. Solar-Driven Carbon Dioxide Reduction: A Fair Evaluation of Photovoltaic-Biased Photoelectrocatalysis and Photovoltaic-Powered Electrocatalysis. *Front. Energy Res.* **2022**, *10*, 956444. [CrossRef]